Spring 2015

Assessment of Electrode Configurations of Electrical Impedance Myography for the Evaluation of Neuromuscular Diseases

Khondokar Mohammad Fazle Rabbi

ASSESSMENT OF ELECTRODE CONFIGURATIONS OF ELECTRICAL IMPEDANCE MYOGRAPHY FOR THE EVALUATION OF NEUROMUSCULAR DISEASES

by

KHONDOKAR MOHAMMAD FAZLE RABBI

ABSTRACT

Electrical impedance myography (EIM) is a painless, noninvasive approach to measure the neuromuscular disease status. EIM parameters- resistance (R), reactance (X) and phase (θ) depend significantly on subcutaneous fat thickness, muscle size and inter electrode distance. The objective of this research is to find an electrode configuration which can minimize the effects on EIM parameters due to subcutaneous fat thickness variation. In this study, a model of human upper arm was developed using finite element method (FEM), which has already been established as an appropriate approach for the analysis of non-symmetrical shape for assessing alternations of muscle in disease-induced changes through EIM. Finite element model with two different kinds of electrode shapes namely rectangular (conventional shape) and circular shapes (proposed shape) were designed for a subcutaneous fat range of 5mm to 25mm. The results show that the standard deviation of reactance values measured for this specified range of fat thickness is 0.65 Ω for circular electrodes, whereas for the rectangular electrode this value is 2.04 Ω. Finally, genetic algorithm was implemented to find an optimized electrode shape which also indicates that the conventional rectangular electrode shape is not the ideal shape for EIM measurements.

ASSESSMENT OF ELECTRODE CONFIGURATIONS OF ELECTRICAL IMPEDANCE MYOGRAPHY FOR THE EVALUATION OF NEUROMUSCULAR DISEASES

by

KHONDOKAR MOHAMMAD FAZLE RABBI

B.S., Bangladesh University of Engineering and Technology, Bangladesh, 2012

A thesis Submitted to the Graduate Faculty of the Georgia Southern University in the Partial Fulfillment of the Requirements for the Degree of

MASTERS OF SCIENCE IN APPLIED ENGINEERING

Statesboro, Georgia

2015

ASSESSMENT OF ELECTRODE CONFIGURATIONS OF ELECTRICAL IMPEDANCE MYOGRAPHY FOR THE EVALUATION OF NEUROMUSCULAR DISEASES

by

KHONDOKAR MOHAMMAD FAZLE RABBI

Major Professor: Mohammad Ahad, PhD

Committee: Rocio Alba Flores, PhD

Danda B Rawat, PhD

Electronic Version Approved:

Spring 2015

DEDICATION

To my beloved family

ACKNOWLEDGEMENTS

First of all I express my profound gratitude to my thesis supervisor, Dr. Mohammad Ahad, Department of Electrical Engineering, Georgia Southern University for enlightening me about the utmost importance of bio-instrumentation. Without his continuous supervision, guidance, thoughtful suggestions and valuable advice, this work would never be possible.

I am grateful to all of those with whom I have had the pleasure to work with during this research. I also thank Somen Baidya, Graduate Assistant, Georgia Southern University. I am extremely grateful and indebted to him for his cooperation as a lab partner.

I also thank to my parents, my wife, my newborn daughter and all family members for their encouragement and love during my course of work.

Lastly, I express my gratitude to GSU library. Many reference papers and books which are necessary for our thesis work have been issued from the library.

TABLE OF CONTENTS

LIST OF FIGURES

LIST OF TABLES

LIST OF SYMBOLS

Symbol	Explanation
R	Resistance
X	Reactance
Θ	Phase
V	Voltage
I	Electric Current
Z	Impedance
σ	Conductivity
ϵ	Permittivity
K	Geometric factor
d	Distance between voltage electrodes
A	Cross-sectional area
Ω	Applied frequency
C	Capacitance
G	Conductance

CHAPTER 1

1 Introduction

1.1 Neuromuscular Disease

Neuromuscular disease affects the nerves that control voluntary muscles. When these nerves are disrupted, it becomes tough or impossible to control the movements of the affected area, such as arms and legs. Several reports suggest that the neuromuscular disease center treats over 2000 people each year. Most of these patients suffer from ALS (Amyotrophic lateral sclerosis), muscle disorders, nerve disorders and myasthenia gravis. Approximately, 5,600 people in U.S.A are diagnosed with this ALS each year and as many as 30,000 may have this disease at any given time.

During the past century, researchers have developed many effective systems of diagnosing neuromuscular diseases using bioelectrical assessments. Though each of these methods has its own advantages in identifying neuromuscular diseases, they also deliver disadvantages in their own ways. Electromyography (EMG), ultrasound and magnetic resonance imaging (MRI) are three main current clinical neuromuscular disease diagnosis techniques.

1.1.1 Electromyography (EMG)

Electromyography has been a settled clinical approach since 1960 (Hardyck 1966). In EMG, a needle is inserted into the muscle which provides valuable insights into the patient's muscle activities. Since the electrodes can measure motor unit potentials at a closer proximity, EMG is usually much more accurate and in depth than electrical impedance myography (EIM). The

electrical activity of the muscle is displayed in the monitor as wavy and spiked lines of voltage over time domain (Kaplanis 2009) may also be heard on a loudspeaker when the muscle is contracted. The whole EMG procedure takes 30 to 60 minutes. EMG recording showing abnormal wave lines when a muscle contracts may mean a muscle or nerve problem, such as a herniated disc, amyotrophic lateral sclerosis (ALS), or inflammation. The main challenge with the EMG is it can be painful and discomforting to the patient and requires a hospital with a specifically designed room where no outside electrical interference can disrupt the results.

1.1.2 Ultrasound

In ultrasound, a transducer sends out a high frequency of sound waves of above human hearing and receives their echoes. The sonographic appearance of the muscle is fairly distinct and can easily be discerned from surrounding fat, bone, nerves and blood vessels (Pillen 2008). Ultrasound has been useful in detecting muscle tears from hematomas within 2 to 48 hours of muscle injury. It also provides good indications in detecting muscle atrophy, inflammation, avulsion and tumors (Peetrons 2002). The main challenge with ultrasound is that it only provides the structure or quality of muscle; it’s hard to interpret any quantitative data from the images.

1.1.3 Magnetic Resonance Imaging (MRI)

MRI is used to scan patients and determine the severity of any disease or injury. MRI uses magnetic field and radio frequency wave to create the detailed 3D images of the entire body. Though MRI is virtually painless, but it is expensive and it can only create images of the general architecture of the muscle, rather than the muscle fiber properties.

As compared to these three procedures, EIM has some major advantages and it is different from these methods of diagnosing neuromuscular disorders in many ways. Unlike EMG, EIM is not highly sensitive to other electrical activities, so it does not require any specially designed room and it is painless. In comparison with MRI which requires the entire body to be scanned, EIM can only examine a single muscle.

1.2 Electrical Impedance Myography

Electric impedance myography (EIM) is impedance based tetra polar technique for the assessment of disease affecting nerve and muscle (Narayanaswami, et al. 2012). This technique is effective for monitoring neuromuscular disease status. High frequency, low intensity electrical current is injected via surface electrode to localized area and the resulting voltage patterns are analyzed (Shiffman, Aaron and Altman 2002). EIM is painless, non-invasive approach which is sensitive to disuse atrophy (Garmirian, Chin and Rutkove 2009).

Resistance (R), reactance (X) and phase (θ) are the three parameters assessed in EIM. Changes in these three parameters occur due to disease (Esper, et al. 2006). These changes are also dependent on number of other factors. For example, size and shape of the muscle and the orientation of muscle fibers both affect the data. There are also some non-muscular anatomic data which impact the data. Subcutaneous fat thickness, choice of electrode and inter-electrode distances are among them. Therefore, if EIM is to be used as a clinical tool, then these electrode parameters have to be standardized (Rutkove, Zhang, et al. 2007).

1.3 Background of this study

Currently many researchers have been working to make EIM suitable for clinical use. Since human tissue was not available, experiments had been performed on rats in three different conditions (normal, acute and chronic). For assessing the relationship between EIM data and the electrical properties of the tissues in rat muscle finite element method (FEM) is employed. Many muscular and non-muscular factors are considered to evaluate the voltage patterns in the sense electrodes. In this research different electrode shapes for a fixed inter-electrode distance have been used to find out the impact on EIM parameters on various temperatures.

1.4 Objective of the Research

The objective of this research is to analyze different electrode configurations to find out the impact on EIM data. In order to refine electrode configuration to optimize EIM for clinical use, following objectives were set for the research

- Design a 3-D model of human upper arm using Comsol Multiphysics 4.3 software.
- Perform the simulation of the model for different electrode shapes.
- Determine which parameter (resistance, reactance and phase) is least affected due to change in subcutaneous fat thickness.
- Propose an optimized electrode shape using genetic algorithm in Matlab.
- Analyse temperature dependency of EIM parameters using Finite Element Model.

1.5 Outline of the Thesis

Chapter 2 Literature Review Elaborately covers the findings of several researchers. It explains the EIM experiment procedures on rats, FEM model of rat leg limb and analysis of the data obtained from previous work.

Chapter 3 Methodology Outlines the methods of this study. It mainly focuses on the Comsol software design of human upper arm with simulation at different conditions.

Chapter 4 Results and Discussions Discusses the results yielded from the FEM model, and proposed electrode configuration from genetic algorithm (ga).

Chapter 5 Conclusion and Scope of Future Work Final conclusion on the current study and based on the laggings it will provide guidance for future studies.

CHAPTER 2

2 Literature Review

2.1 Electrical Impedance Myography (EIM) Experiment

Electrical impedance myography (EIM) is a non-invasive, painless electrophysiological approach to muscle assessment based on the application and measurement of high frequency, low intensity electrical current. Low amplitude electrical current is applied via surface electrodes over discrete areas of muscle and the corresponding voltage patterns are analyzed for the assessment of neuromuscular disease. Conventional needle approach electro-myography (EMG) focus on the inherent electrical activity of the tissues, but in EIM measurements are taken over a small area of interest and it also depends on the changes in the composition and structure of the muscle that accompany neuromuscular disease (Ahad, Fogerson, et al. 2009). EIM is still the stage of development but it can be a major indicator of neuromuscular disease status and as a diagnostic tool (Rutkove 2009).

Three major parameters assessed in EIM include resistance (*R),* reactance *(X)* and phase *(θ)*. Significant changes in these parameters occur due to muscle composition change with disease progression (Jafarpoor, et al. 2013). The value of these parameters depends not only on the weak electrical current through muscle tissue, but it also depends on many other factors. The shape and size of the muscle, even the orientation of muscle fiber influences the data. Because muscle fiber is anisotropic, current flows in both longitudinal and transverse direction (Wang, et al. 2011). Non-muscular anatomic factors also impact the data. The major factor among those which

impacts the data significantly is subcutaneous fat thickness (Sung, et al. 2013). Finally these parameters are highly dependent on the shape of the electrodes and inter-electrode distances.

Everything that lies under and between the electrodes contributes to the measured impedance of the biological tissue. This impedance depends on the basic principle that, if an alternating current is applied, energy will be dissipated as it travels through it, thus producing the measuring voltage. Mathematically it can be expressed by the Ohm's law:

$$V=IZ \tag{1}$$

Where V is voltage, I is current flow and Z is the impedance. Measured complex impedance from the experiment can be written as

$$Z=R + jX \tag{2}$$

So, the complex admittance becomes

$$Y = \frac{1}{Z} = G + jwC \tag{3}$$

Where G is the conductance and capacitance is C

Here, $G = \frac{R}{R^2+X^2}$ and $C = \frac{X}{(R^2+X^2)w}$

So the muscles internal electrical property, conductivity and relative permittivity depend on conductance, capacitance and geometric factor. So the conductivity, $\sigma = K.\ G$

And the relative permittivity, $\epsilon_r = \frac{K.C}{\epsilon}$, where K is the geometry factor of muscle = $\frac{d}{A}$. Here d is the distance between voltage electrodes and A is cross sectional area of the muscle.

Muscles are made up of long bundled parallel fibers that have the ability to conduct electricity due to the biological properties of tissues. Healthy muscles are organized in an anisotropy manner meaning electric current flows easily along the muscle fiber rather than across them (Aaron, Huang and Shiffman 1997), but as neurogenic disease disorganizes fiber structure and replaces it with fatty tissue, the muscle tends to demonstrate isotropic properties resulting in

disturbed impedance values. Everything that lies under and between the electrodes contributes to the measured impedance of a muscle, including a highly conductive saline solution. Various concentrations of intracellular and extracellular fluids along the muscle membranes will cause a change in lipid bilayers of muscles. These bilayers act as additional capacitors that will store and release charge with the reversing current flow during isometric contractions (Rutkove, Zhang, et al. 2007). Rutkove illustrates a simplified '3-element' circuit diagram of muscle tissue for the theory of electrical impedance in Figure 1.

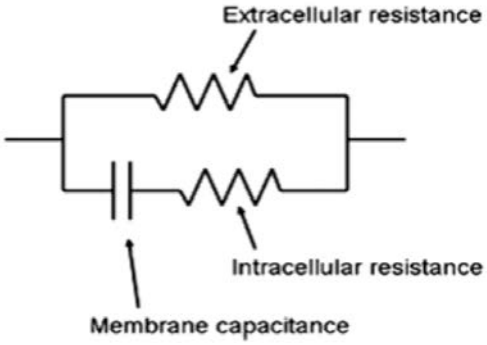

Figure 1: Muscle Tissue Circuit Diagram (Rutkove, Zhang, et al. 2007)

The capacitor represents the reactance of cell membranes and the resistors represent the extra and intracellular resistance of a skeletal muscle. Moreover, the capacitance varies on the frequency of the applied current, which in turn fluctuate the reactance of each muscle tissue. At lower frequencies, the current will flow initially through all three elements until the capacitor is fully charged. Once charged, the current will only flow across the extracellular resistor, but at higher frequencies of alternating currents, the current will be able to penetrate both the extra and intracellular resistors. The mathematical relationship of frequency (in Hz), resistance, and capacitance is

$$f_{peak} = \frac{1}{R_i + R_e C^2} \tag{4}$$

Here, R_i is the intracellular resistance and R_e is the extracellular resistance.

Significantly higher frequency values make the capacitance of cell membranes virtually obsolete, thus contributing to little change in impedance measurements. Previous studies to date have concluded that a frequency of 50 kHz is sensitive enough to detect neurogenic and myopathic diseases using EIM (Shiffman, Aaron and Altman 2002). As a result, much devoted research has been focused at 50 kHz, but using measurements over a full frequency spectrum will still produce contributable data to the field.

Several experiments have been performed so far to validate the effectiveness of EIM. Since human tissue was not available for acute and crush conditions, muscle was obtained from rats (Jafarpoor, et al. 2013).

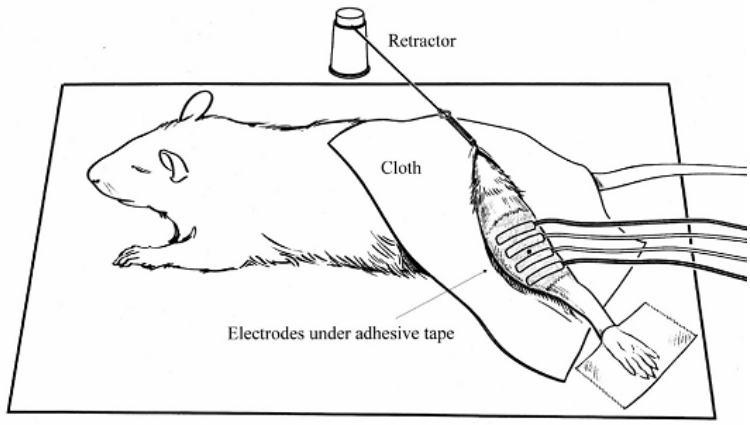

Figure 2: Rat EIM measurement set-up (Ahad and Rutkove 2009)

Previous results demonstrate that impedance values are outstandingly consistent over time when animals reach approximately 14 weeks of age. But during the growth phase, the values of resistance and reactance decrease. Also if the girth is increased this implies a larger muscle volume, then the value of resistance and reactance decreases. However despite minimal weight

gain and leg girth enhancement after 14 weeks, EIM values remain almost stable (Ahad and Rutkove 2009).

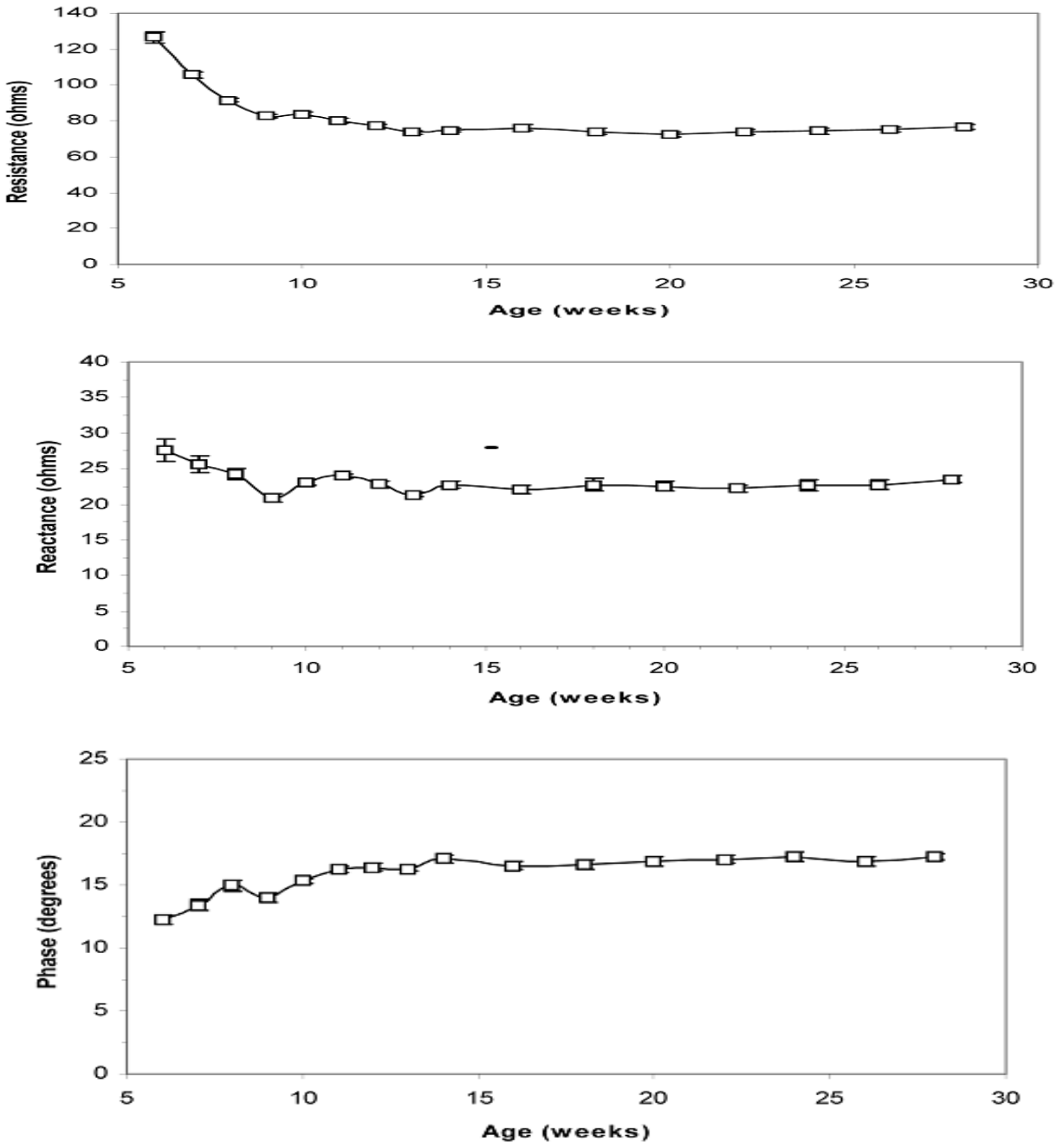

Figure 3: Resistance, reactance and phase data of the rats, from 6 weeks of age onward. Note gradual reduction in reactance and resistance up to approximately 14 weeks of age, followed by excellent stability over the ensuing several months (Ahad, Fogerson, et al. 2009)

However researchers found out later that, after sciatic crush the values of these parameters are consistent with human disease work. Here the values of phase and reactance decreases but resistance increases. Acute conditions are severe and sudden in onset. This could describe anything from a broken bone to an asthma attack. A chronic condition, by contrast is a long-developing syndrome, such as osteoporosis or asthma.

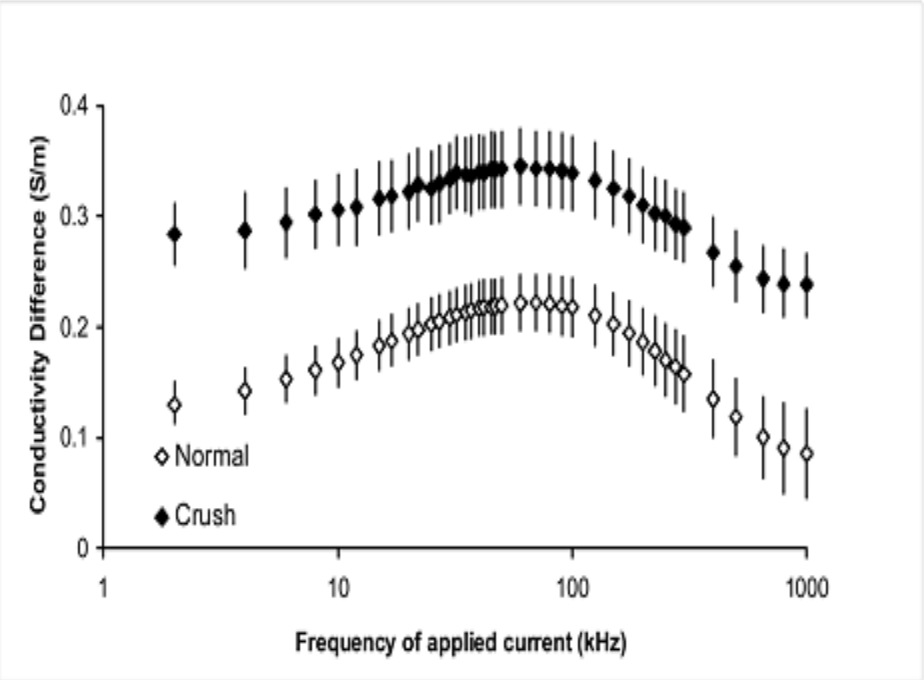

Figure 4: Conductivity differences in normal and sciatic crush animals from 2 kHz to 1 MHz (Ahad and Rutkove 2009)

One of the major factors which are considered during obtaining the value of the impedance is the electrical anisotropy of muscle fiber. Previous findings demonstrate significant conductivity difference and relative permittivity difference between healthy rats and rats those went under sciatic nerve crush (Ahad and Rutkove 2009).

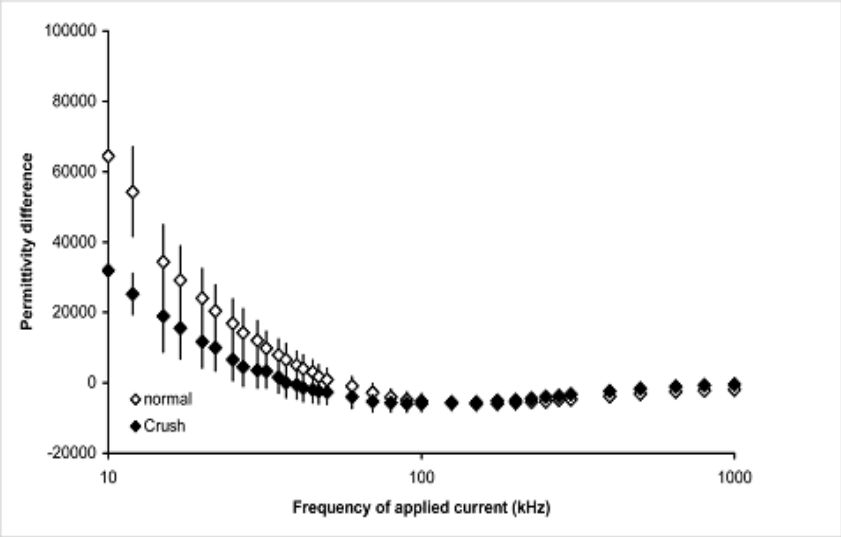

Figure 5 Relative permittivity differences in normal and sciatic crush animals from 2 kHz to 1 MHz (Ahad and Rutkove 2009)

2.2 Finite Element Method

The rat hind model was developed using the AC/DC Module, Electric Current Physics, in Comsol Multiphysics software (Comsol, Inc, 4.3a, Burlington, MA). To make the model more accurate MRI images of the rat hind leg is used (Wang, et al. 2011). The model consisted of several layers, skin/subcutaneous layer, fat layer, a fascia layer, two bones (tibia and fibula), the biceps femoris, the gastrocnemius-soleus complex, and the tibialis anterior. Small angles are used to represent the slight offset in muscle fiber direction from parallel. Thickness of the subcutaneous fat is measured 1 mm and the fascial layer 0.5 mm. Only the metallic surface of the electrode is modeled where the dimension is 3.5 mm x 1.8 mm. The boundary condition is a critical part where it is considered that no current flow out of any exterior boundaries, only the part under the electrode is conductive. The value of conductivity used for subcutaneous fat is 0.03 S/m and for the fascia layer 0.2 S/m. For bone, conductivity is assigned 0.02 S/m and relative permittivity 6000. The electrodes conductivity and relative permittivity value are set to

5.0e5 S/m and 1.0 respectively. Frequency analysis is also performed within a range of 10 kHz to 3 MHz (Wang, et al. 2011).

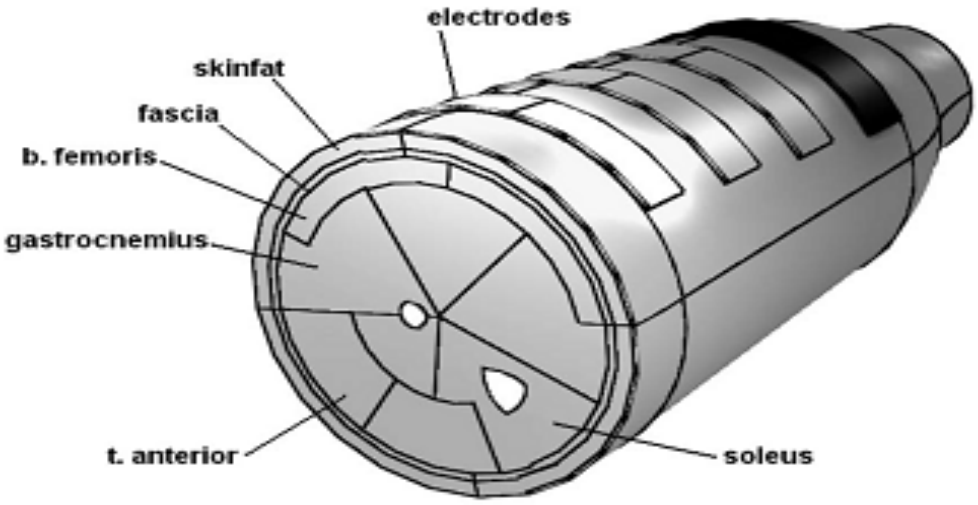

Figure 6: FEM model of chronic crush rat hind leg (Wang, et al. 2011)

Using the finite element method described in previous publication, values obtained from this method is compared with the EIM measurements for 50 kHz. An internal check was also performed to make the measurements more precise.

Table 1: Comparison between EIM measured values and FEM model at 50 kHz (Wang, et al. 2011)

EIM			
Value	**Normal**	**Acute**	**Chronic**
R50	73.3±0.9	74.2±1.9	72.7±3.2
X50	22.8±0.2	18.2±0.6	21.2±1.2
P50	17.3±0.3	13.8±0.7	16.1±0.5

FEM			
Value	**Normal**	**Acute**	**Chronic**
R50	86.7	87.8	78.3
X50	36.7	29.9	30.3
P50	24.3	18.8	21.2

Multi-frequency spectrum is also plotted using FEM and the dielectric data obtained from earlier publications on rat experiments. The frequency range selected for this experiment was from 10 kHz to 4 MHz. Frequency analyses is performed over all the three cases: normal, acute and chronic. Average girth at the midpoint of the electrode array was included in the model.

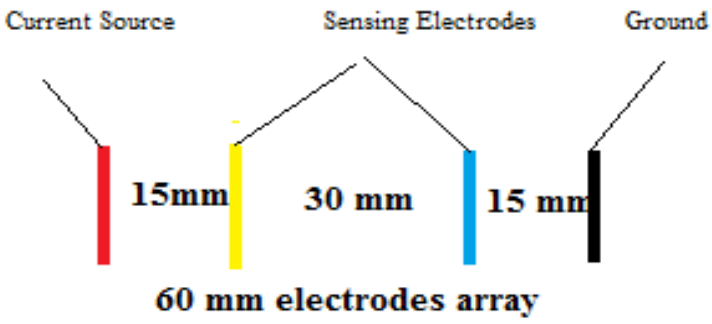

It took 20 s within 1 e-3 Ω of the convergence limit to finish the impedance calculations using finite element method. Here the surface impedance values of the chronic group and the normal group are almost similar. The reason behind this is the 6 months post-surgery recovery period (Wang, et al. 2011).

To summarize the spectrum nature, collapsed parameters (logRslope, the reactance slope and the phase slope) were also utilized (Wang, et al. 2011). Here predicted values were shown just below the measured value for all three normal, acute and chronic conditions. It is clear from figure 7 and 8 that FEM predicted outcomes were parallel to EIM measurements, except for the case of 50 kHz reactance for the chronic crush and phase slope for the acute crush animals (Wang, et al. 2011).

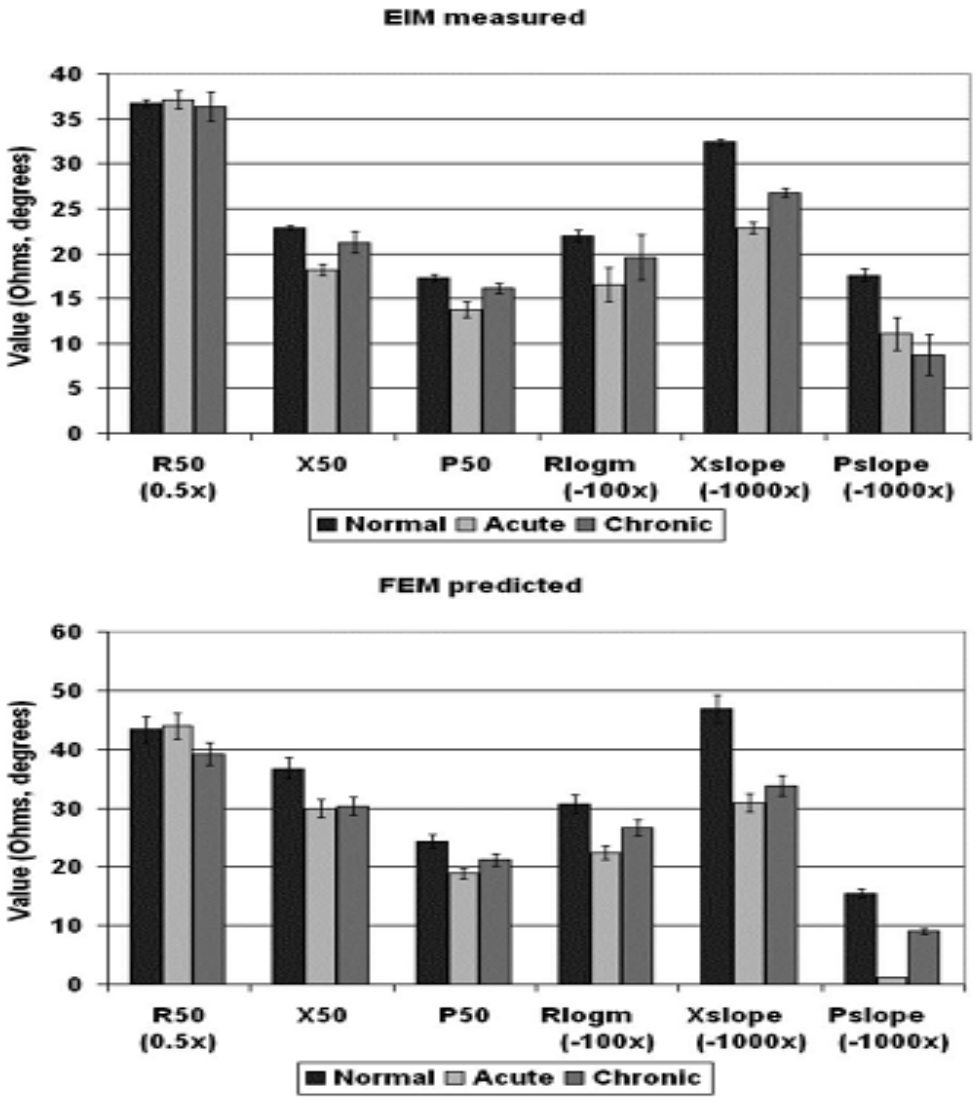

Figure 7: Comparative bar chart for all three conditions for both EIM measured values and FEM predicted values (Wang, et al. 2011)

The reason behind these inconsistencies is the measured value of the conductivity and permittivity of the tissue. Because these values are highly sensitive to moisture, temperature, quality of tissue after death, cross-sectional area and most significantly distance between voltage measuring electrodes during measurements (Wang, et al. 2011).

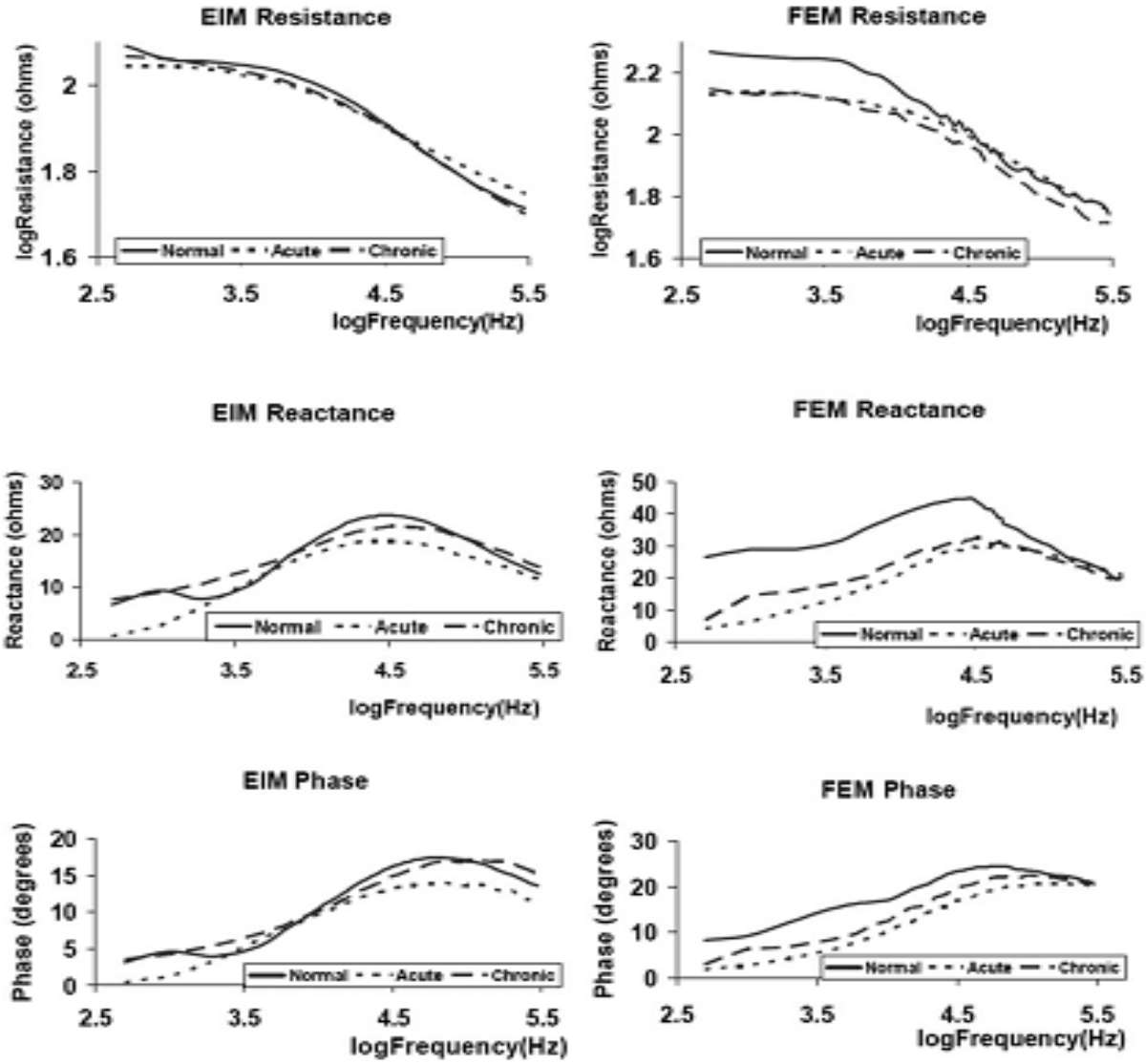

Figure 8: Average EIM resistance, reactance and phase next to the counterparts predicted by using FEM (Wang, et al. 2011)

EIM measurements are also performed on human. Here the surface impedance values and subcutaneous fat thickness are taken from a 47 year old healthy male.

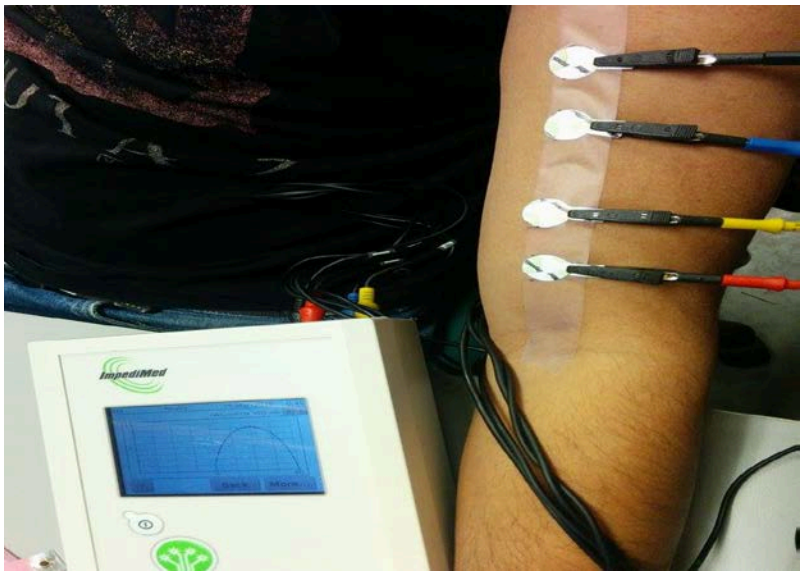

Figure 9: EIM experiment on human subject

But the dielectric data of muscle tissue is taken from the rats (Jafarpoor, et al. 2013).

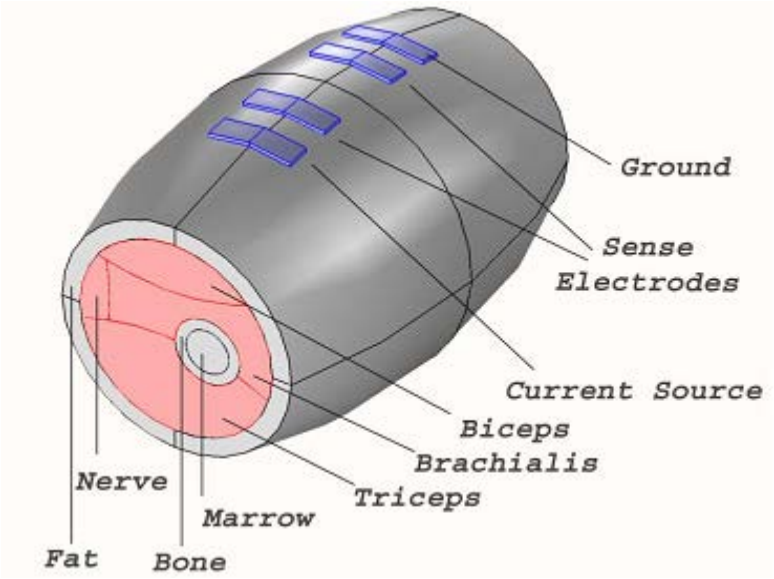

Figure 10: FEM model of the human arm using Comsol Multiphysics 4.2a based on anatomic data. Inter-electrode spacing 15-30-15 mm (Jafarpoor, et al. 2013)

Multi-frequency measurements were performed with an ImpediMed SFB7 ® device (ImpediMed, Inc., Queensland, Australia. http://www.impedimed.com). This single channel, tetra polar bioimpedance spectroscopy (BIS) device scanned 256 frequencies between 4 kHz and 1000 kHz. The device was chosen for its reliability, portability, and ease of use in the biomedical field. Each measurement took less than three seconds to compute resistance (R), reactance (X), and impedance (Z) graphs that were stored directly on the instrument. Phase (θ) was calculated using the corresponding equation at each frequency. A software illustration and its corresponding graphs can be seen in Figure 11.

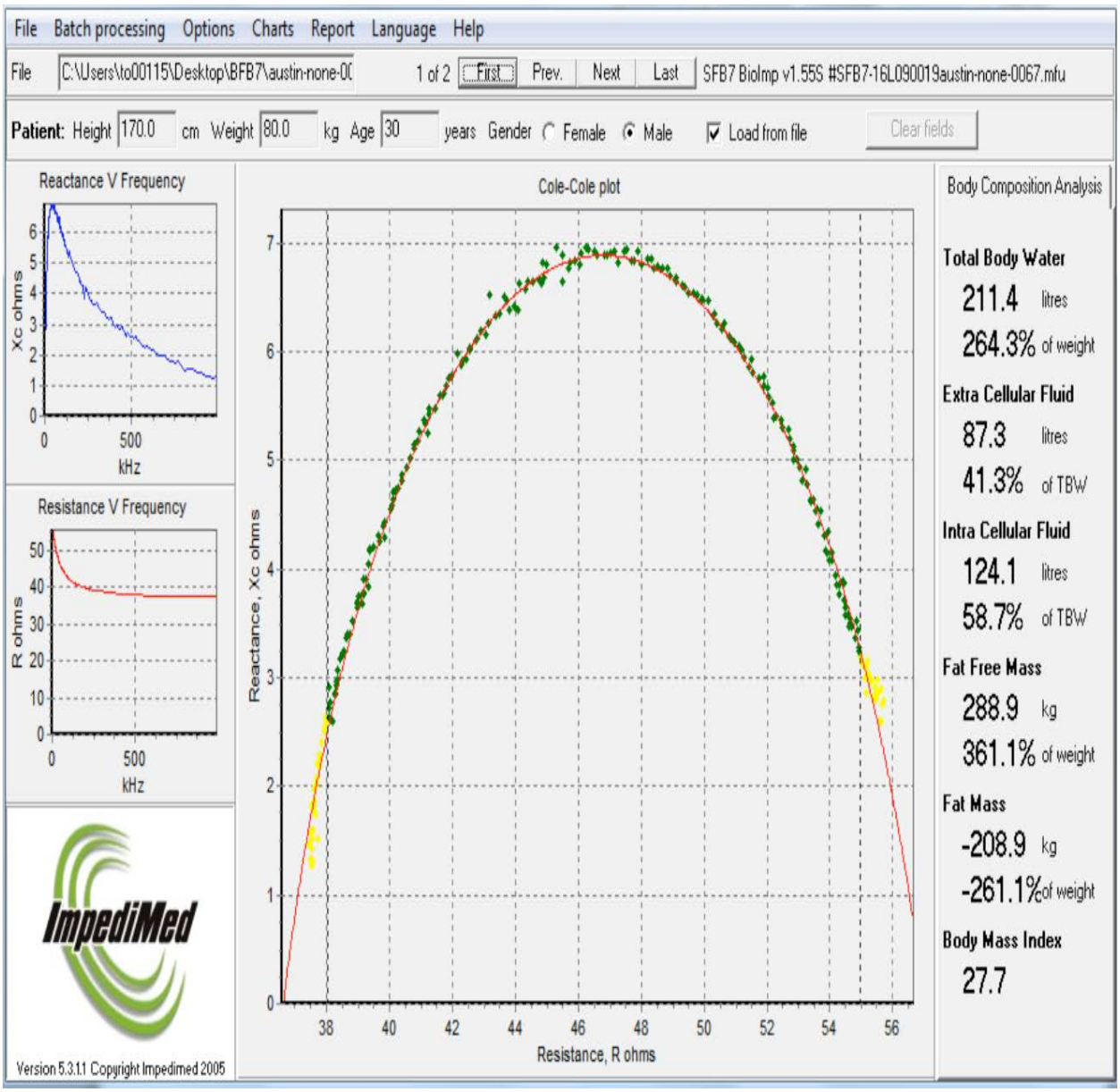

Figure 11: Cole-cole plot from EIM experiment

Several variation of this model is made to find out effects on resistance, reactance and phase. Surface recorded human data and FEM generated data is compared. It is shown in the fig. 12 that though the curves are similar but there is slight offset for both the reactance and the phase angle values (Jafarpoor, et al. 2013)

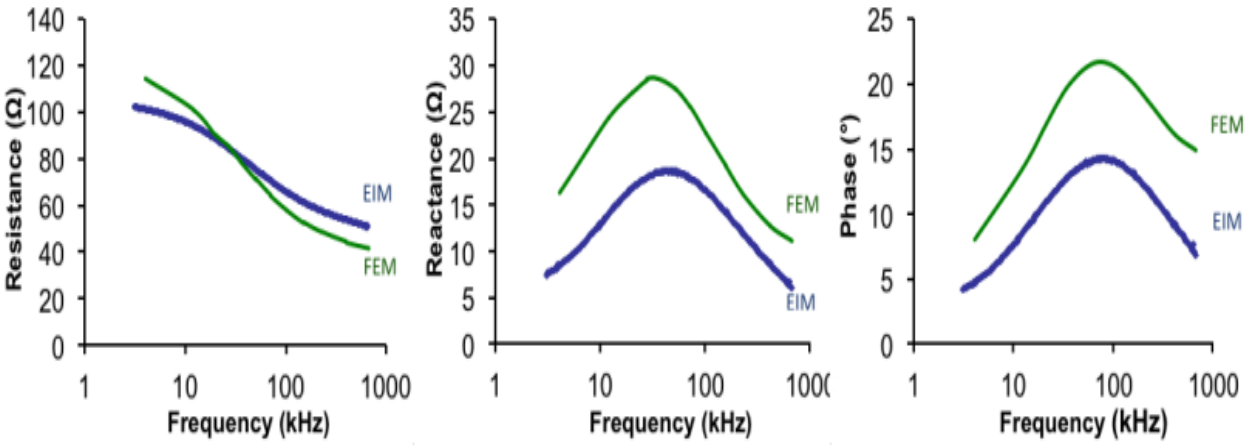

Figure 12: Comparison of EIM data from 47 year old healthy male volunteer (blue line) and that generated using FEM (green line) (Jafarpoor, et al. 2013)

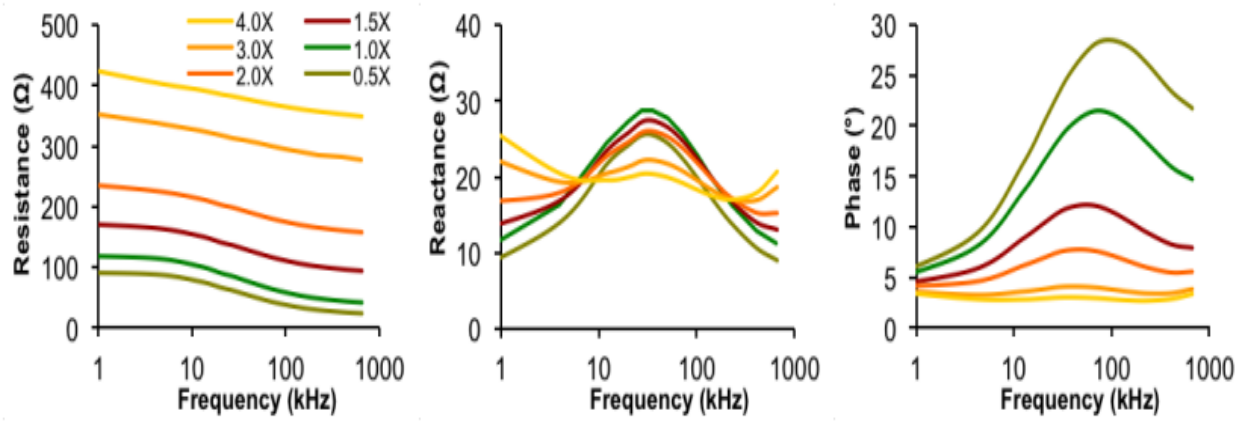

Figure 13: The effect of altering the baseline 4.4 mm subcutaneous fat thickness on the resistance, reactance and phase. (Jafarpoor, et al. 2013)

It is also observed from fig. 13 that subcutaneous fat thickness affect the data significantly. Resistance and phase shows strong dependence on skin subcutaneous fat thickness over the whole frequency spectrum, but in case of reactance considerably smaller changes are noticeable (Jafarpoor, et al. 2013).

Another important factor which is also considered is the effect of altering muscle size, because this type of variation is observed in healthy individuals. Here in fig. 14, the measurements are

substantially impacted only if the muscle size is reduced to one half of its original size and impact on phase values are very less (Jafarpoor, et al. 2013).

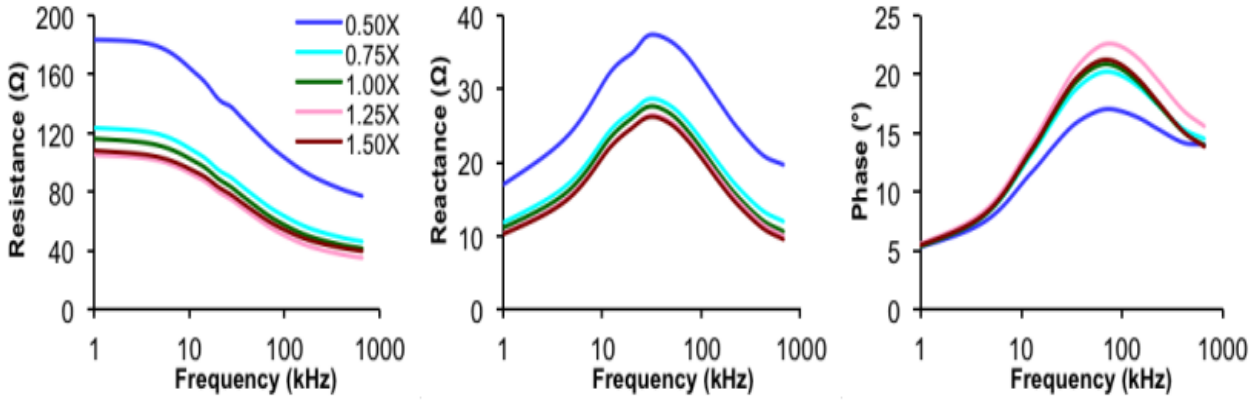

Figure 14: The effect of altering the thickness of muscle on the resistance, reactance and phase using the electrode configuration and spacing shown in fig 8 (Jafarpoor, et al. 2013)

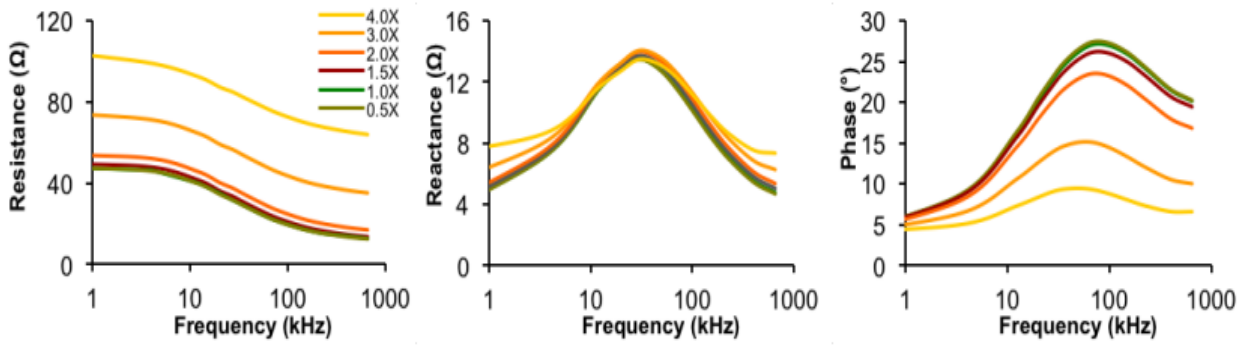

Figure 15: Effect of altering subcutaneous fat thickness with each excitation electrode placed 2 cm further away from sense electrode while keeping the sense inter electrode distance unchanged at 30 mm (Jafarpoor, et al. 2013)

As it is mentioned earlier that optimizing electrode configuration might impact the data greatly. Different electrode spacing is used to perform the same operation where the distance between the sense electrodes is 35 mm, making the length of the entire array 100 mm. It is demonstrated in fig. 15 that in this spacing subcutaneous fat thickness has small effects on resistance and phase and modest difference in reactance values. But the effect on muscle size for this spacing is highly

noticeable in fig 16. The values of all three parameters are larger than the last spacing (Jafarpoor, et al. 2013).

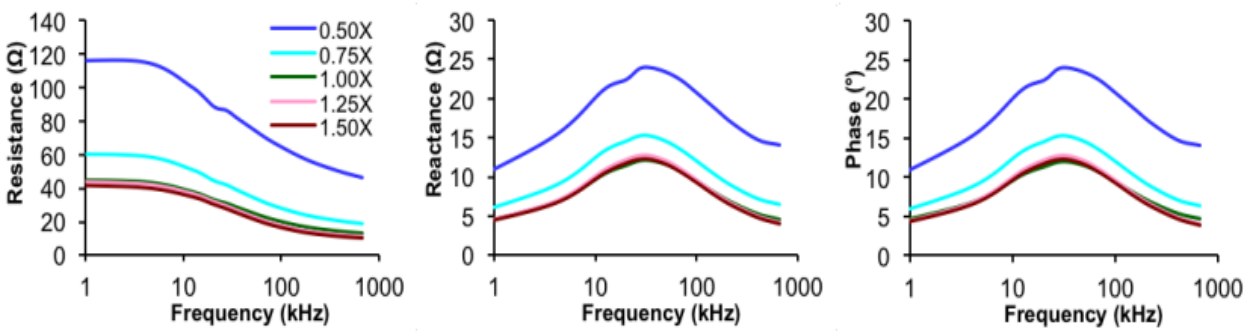

Figure 16: The effects of altering muscle thickness at the greater inter electrode distances (Jafarpoor, et al. 2013)

For different electrode spacing current densities are measured, where it is shown that considerably larger volume through which the current flows if the electrodes are spaced further apart.

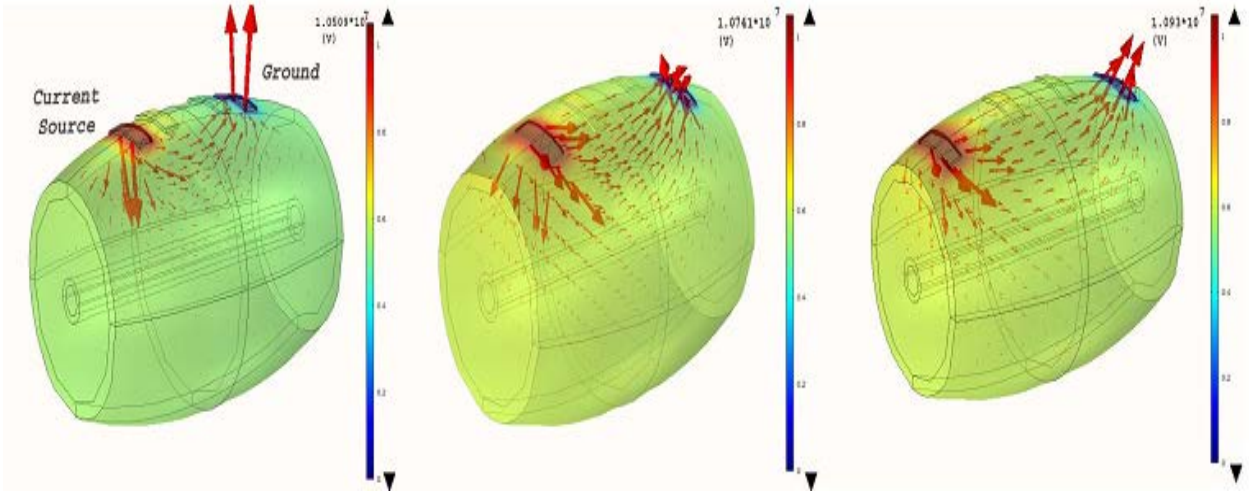

Figure 17: Comparison of current distribution for the three different electrode configurations (14-30-15 mm, 25-30-25 mm, and 35-30-35 mm) (Jafarpoor, et al. 2013)

But larger spacing between electrodes has some drawbacks. A large number of muscles could not be measured because of the larger spacing between the electrodes and another vital drawback is it is not possible to measure the anisotropy properties of muscle. However, if small electrode spacing is considered then the effects of subcutaneous fat thickness on the data plays a vital role. So an optimized electrode configuration is mandatory to perform EIM operation.

CHAPTER 3

3 Methodology

The main objective of this study was to analyze the impacts on EIM parameters due to different electrode configurations and find out the least affected parameter that can detect neuromuscular diseases and at the same time does not vary a lot with different subcutaneous fat thickness. The objective of this study was validated using different approaches. The finite element model (FEM) of human upper arm was designed for different electrode configuration. Then the FEM simulation result was substantiated further using genetic algorithm (ga). Also, changes in EIM parameters due to ambient temperature with different subcutaneous fat thickness were analyzed using finite element method (FEM).

3.1 Finite Element Model (FEM) of Human Upper Arm

Human upper arm model was developed using the AC/DC Module, Electric Current Physics, in Comsol Multiphysics software (Comsol, Imc, 4.3a, Burlington, MA). The model consisted of five layers, skin/subcutaneous fat layer, muscle fiber layer, bone layer and four electrodes. The human upper arm cross sectional view and the corresponding FEM model used for this study is illustrated in Figure 18 and 19 respectively.

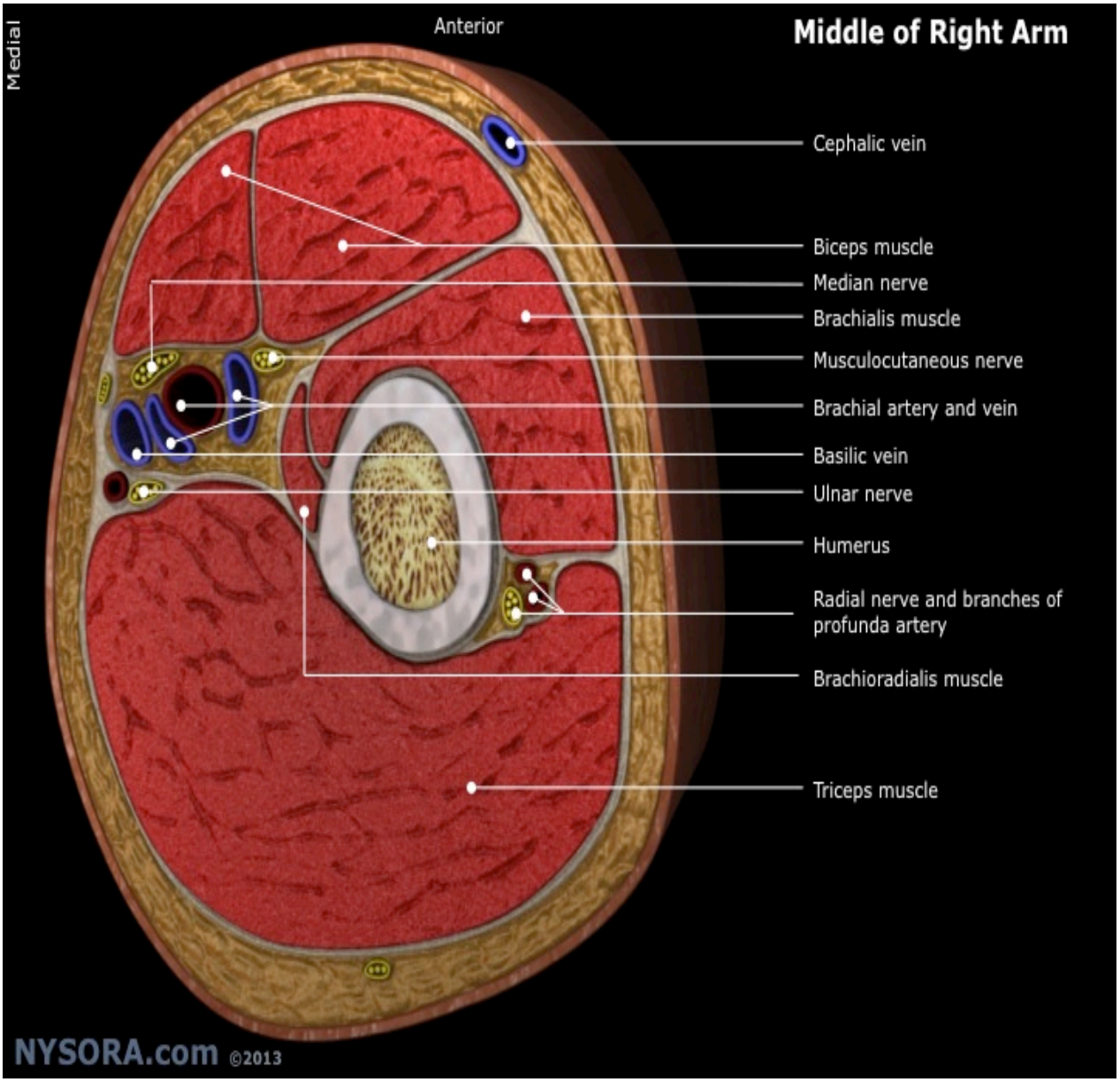

Figure 18: Cross-section through the middle of upper arm (nysora.com n.d.)

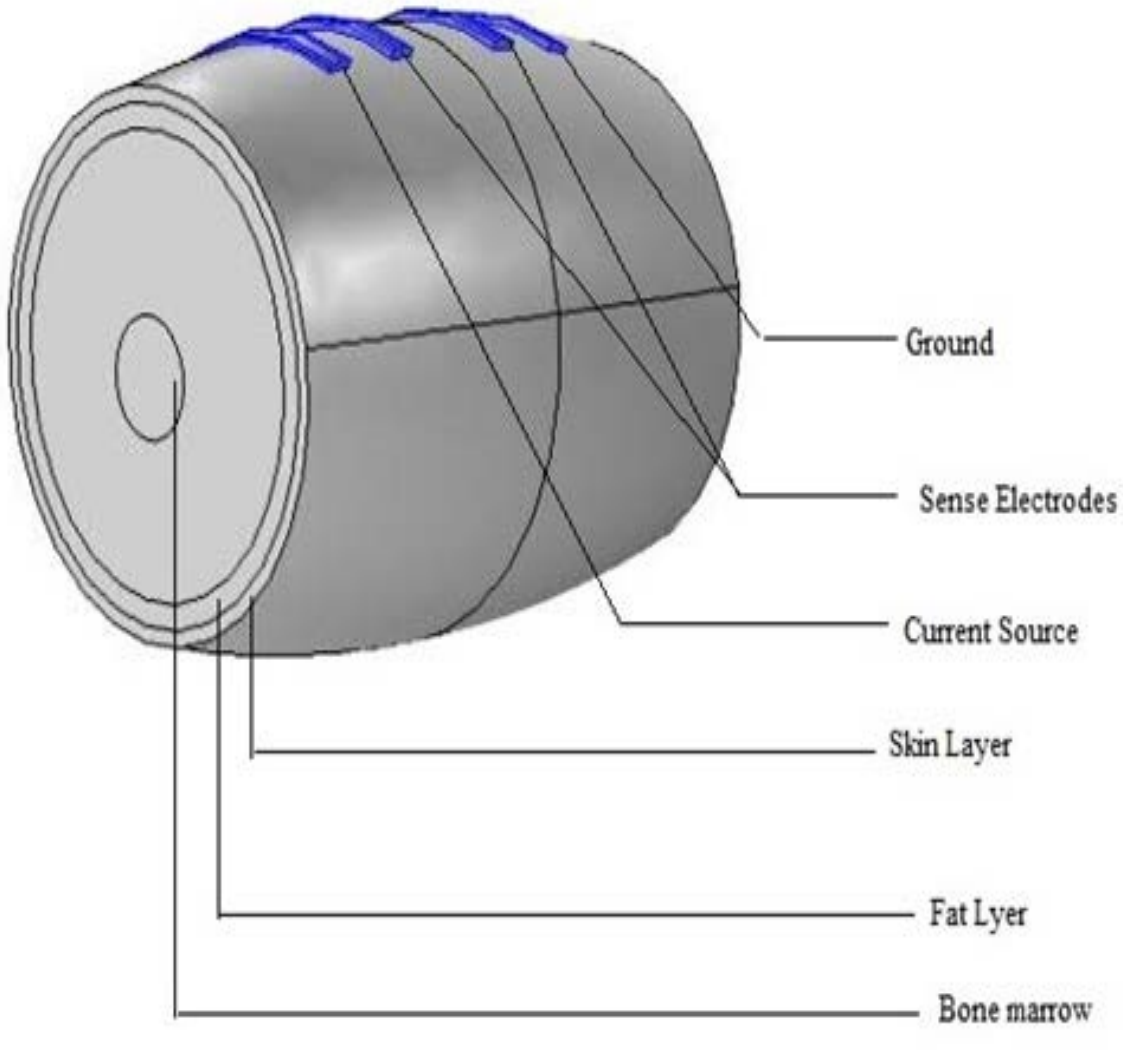

Figure 19: FEM model of the human upper arm using Comsol Multiphysics 4.2a (elbow to axilla) based on anatomic data. The inter-electrode spacing was 15 mm-30 mm-15 mm (60 mm in total)

The skin thickness considered for the model is 3 mm. As the value of the EIM parameters (resistance, reactance and phase) change with the subcutaneous fat thickness, the model was designed for different fat thickness ranging from 10 mm to 24 mm and a fixed muscle fiber thickness of 22 mm. Previous studies suggest that the EIM parameters are very sensitive to

electrode configuration. In this model both the rectangular and circular shape of the electrodes were designed. The rectangular electrode dimension was 25 mm x 7 mm and for the circular electrode the radius was 7 mm. For the both the rectangular and circular electrode, total skin area covered by the electrode was kept same, which is 154 mm^2. Rutkove *et al* suggest that EIM parameters depends on the inter electrode distances. For this study, the inter-electrode distance (edge to edge) for both the circular and rectangular shapes were kept 15 mm-30 mm-15 mm, which is low because higher inter electrode does not consider the anisotropy properties of muscle. The boundary condition was a critical part where it was considered that no current flow out of any exterior boundaries, only the part under the electrode was conductive. The value of conductivity and relative permittivity for different layers at each different frequency were obtained from the published sources. The electrodes conductivity and relative permittivity value were set to 5.0e5 S/m and 1.0 respectively. Out of the four electrode, two exterior electrodes were used an excitation current source of 1 mA and a ground, the other two were voltage sensing electrodes. In this model, the skin-subcutaneous fat and bone were all assumed to be isotropic, where the muscle fiber was anisotropic. A complete mesh of the geometry consisted of 47188 elements.

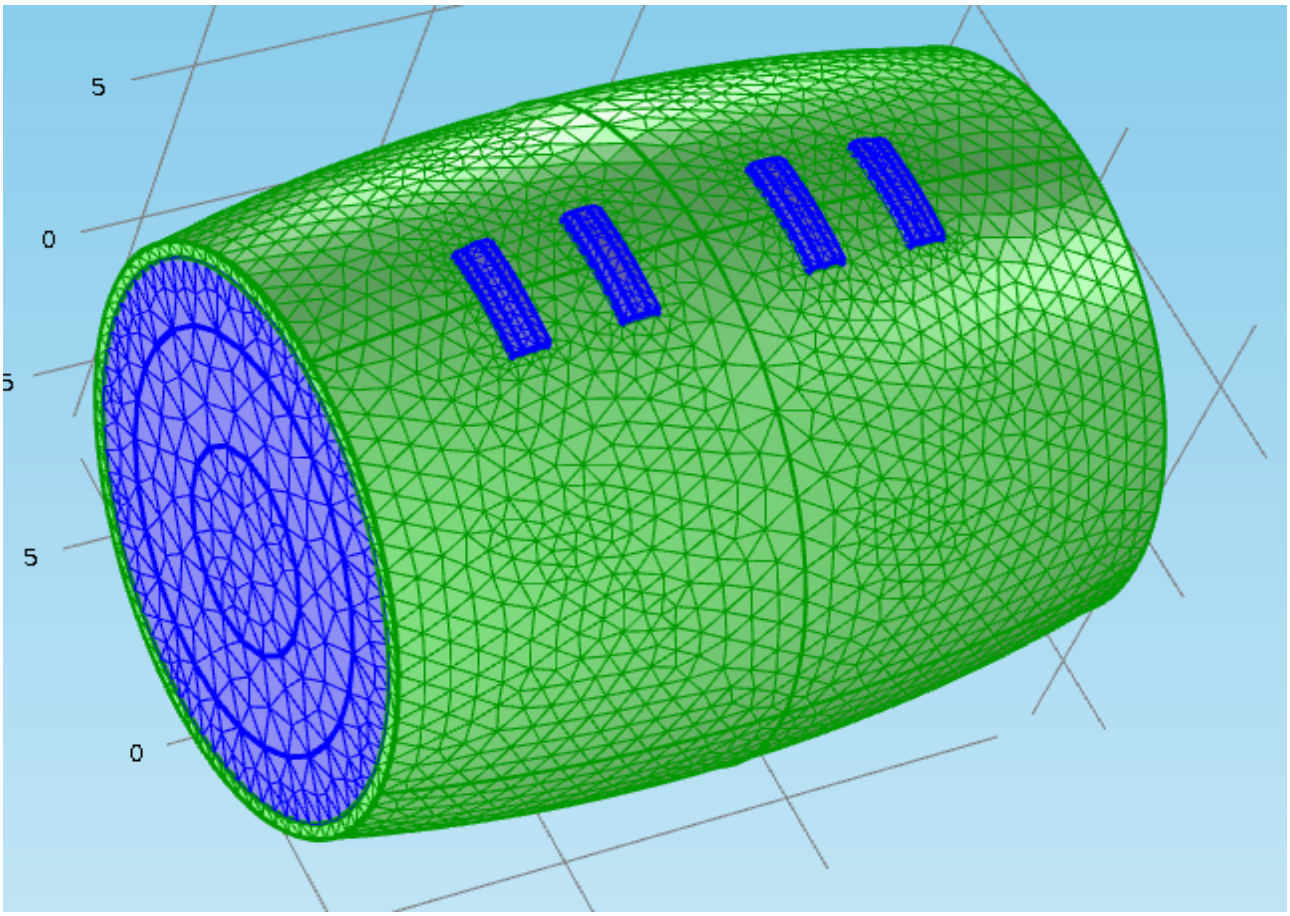

Figure 20: Complete mesh of geometry of human upper arm

The conductivity and relative permittivity values of the skin, fat and bone remains same for three different normal, acute and chronic crush conditions. Acute conditions are severe and sudden in onset. This could describe anything from a broken bone to an asthma attack. A chronic condition, by contrast is a long-developing syndrome, such as amyotrophic lateral sclerosis (ALS) or asthma. The values of the muscle dielectric properties were incorporated from the published sources. (Ahad, Fogerson, et al. 2009).

Table 2: Dielectric Properties of different layers at different conditions

		Normal Tissue		Acute Crush		Chronic Crush	
Frequency	Tissue	Conductivity (S)	Relative Permittivity	Conductivity (S)	Relative Permittivity	Conductivity (S)	Relative Permittivity
10k	Skin	0.0002	1150	0.0002	1150	0.0002	1150
	Fat	0.025	1000	0.025	1000	0.025	1000
	Muscle	{.4, .17, .17}	{120E3, 86E3, 86E3}	{.5, .14, .14}	{104E3, 80E3, 80E3}	{.52, .15, .15}	{126E3, 102E3, 102E3}
	Bone	0.002	675	0.002	675	0.002	675
50k	Skin	0.0002	1150	0.0002	1150	0.0002	1150
	Fat	0.03	500	0.03	500	0.03	500
	Muscle	{.45, .2, .2}	{70E3, 55E3, 55E3}	{.58, .2, .2}	{41E3, 48E3, 48E3}	{.65, .23, .23}	{55E3, 59E3, 59E3}
	Bone	0.0035	300	0.0035	300	0.0035	300
100k	Skin	0.0002	1150	0.0002	1150	0.0002	1150
	Fat	0.03	300	0.03	300	0.03	300
	Muscle	{.55, .3, .3}	{40E3, 36E3, 36E3}	{.65, .2, .2}	{26E3, 36E3, 36E3}	{.73, .32, .32}	{35E3, 44E3, 44E3}
	Bone	0.0035	110	0.0035	110	0.0035	110
1M	Skin	0.02	990	0.02	990	0.02	990
	Fat	0.05	150	0.05	150	0.05	150
	Muscle	{.65, .4, .4}	{4E3, 3E3, 3E3}	{.8, .3, .3}	{2E3, 1E3, 1E3}	{.92, .44, .44}	{3E3, 4E3, 4E3}
	Bone	0.004	40	0.004	40	0.004	40

The sensing electrodes voltage patterns were studied for a frequency range of 10 kHz to 1 MHz. After the simulation the current density throughout the upper arm is given in Fig 21.

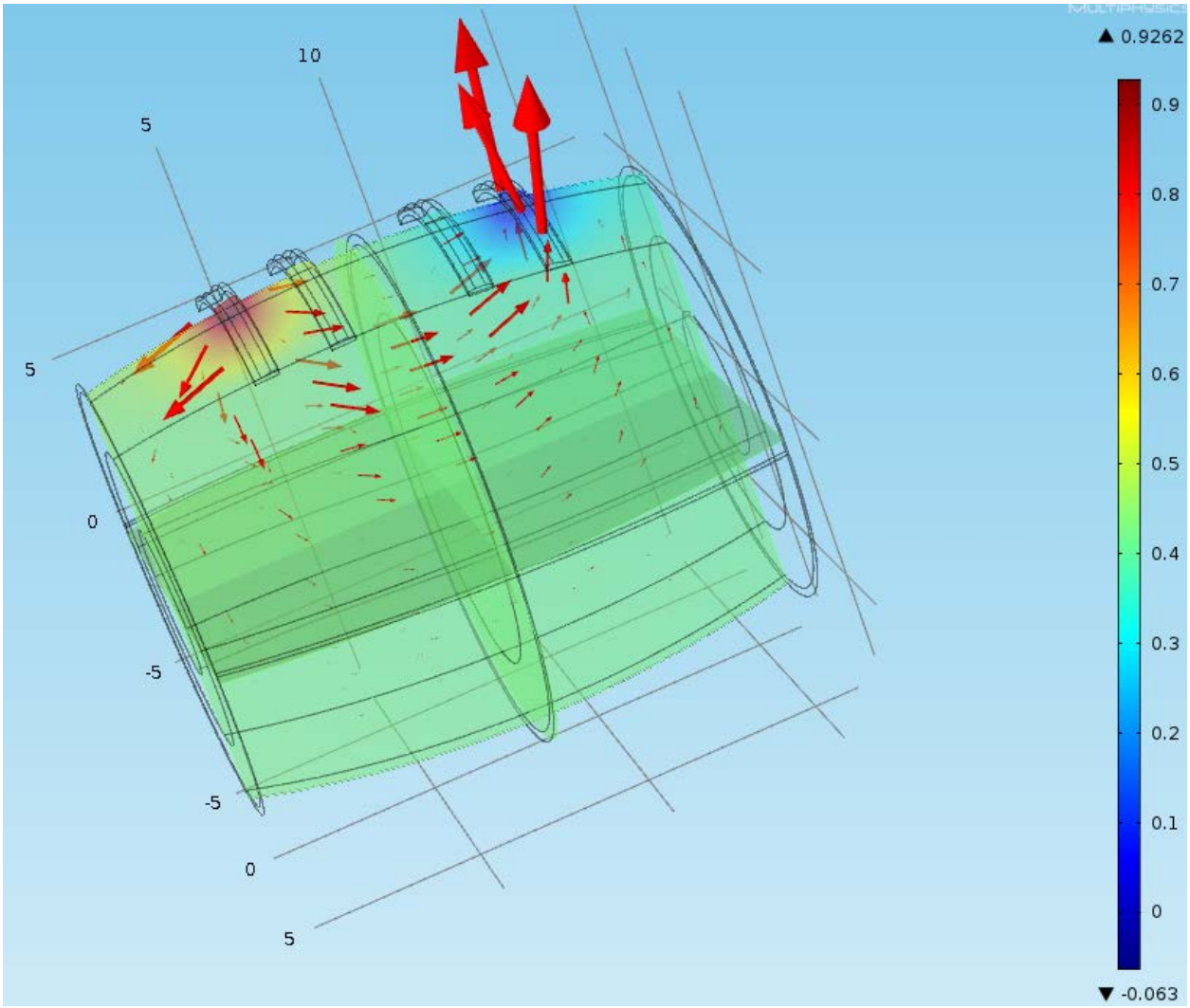

Figure 21: Current density inside the upper arm

3.2 Electrode Shape Using Genetic Algorithm

Genetic Algorithms (GAs) are adaptive methods which may be used to solve search and optimization problems. They are based on the genetic processes of biological organisms. Over many generations, natural populations evolve according to the principles of natural selection and survival of the fittest, first clearly stated by Charles Darwin in The Origin of Species. By mimicking this process, genetic algorithms are able to evolve solutions to real world problems, if they have been suitably encoded. At each step, the genetic algorithm randomly selects individuals from the current population and uses them as parents to produce the children for the next generation. Over successive generations, the population "evolves" toward an optimal solution. For example, GAs can be used to design bridge structures, for maximum strength/weight ratio, or to determine the least wasteful layout for cutting shapes from cloth. They can also be used for online process control, such as in a chemical plant, or load balancing on a multi-processor computer system.

The following outline summarizes how the genetic algorithm works:

1. The algorithm begins by creating a random initial population.
2. The algorithm then creates a sequence of new populations. At each step, the algorithm uses the individuals in the current generation to create the next population. To create the new population, the algorithm performs the following steps:
    a. Scores each member of the current population by computing its fitness value.
    b. Scales the raw fitness scores to convert them into a more usable range of values.
    c. Selects members, called parents, based on their fitness.

d. Some of the individuals in the current population that have higher fitness are chosen as *elite*. These elite individuals are passed to the next population.

e. Produces children from the parents. Children are produced either by making random changes to a single parent—*mutation*—or by combining the vector entries of a pair of parents—*crossover*.

f. Replaces the current population with the children to form the next generation.

3. The algorithm stops when one of the stopping criteria is met, such as generations, time limit, fitness limit, stall test, function tolerance etc.

The purpose of using genetic algorithm in this study is to find the optimized shape of the electrode for which the value of reactance changes least with different subcutaneous fat thickness. Both the COMSOL simulation and EIM experiment show better result for circular shape instead of rectangular shape. To further improve the shape of the electrodes GA algorithm was used. The function of the fitness function used for GA algorithm in this study is to minimize the difference between reactance values for a subcutaneous fat thickness range of 10 mm to 25 mm. The variable used for the optimization was angle within a range of 15^0 to 360^0. A software illustration of the genetic algorithm is given in Fig 22.

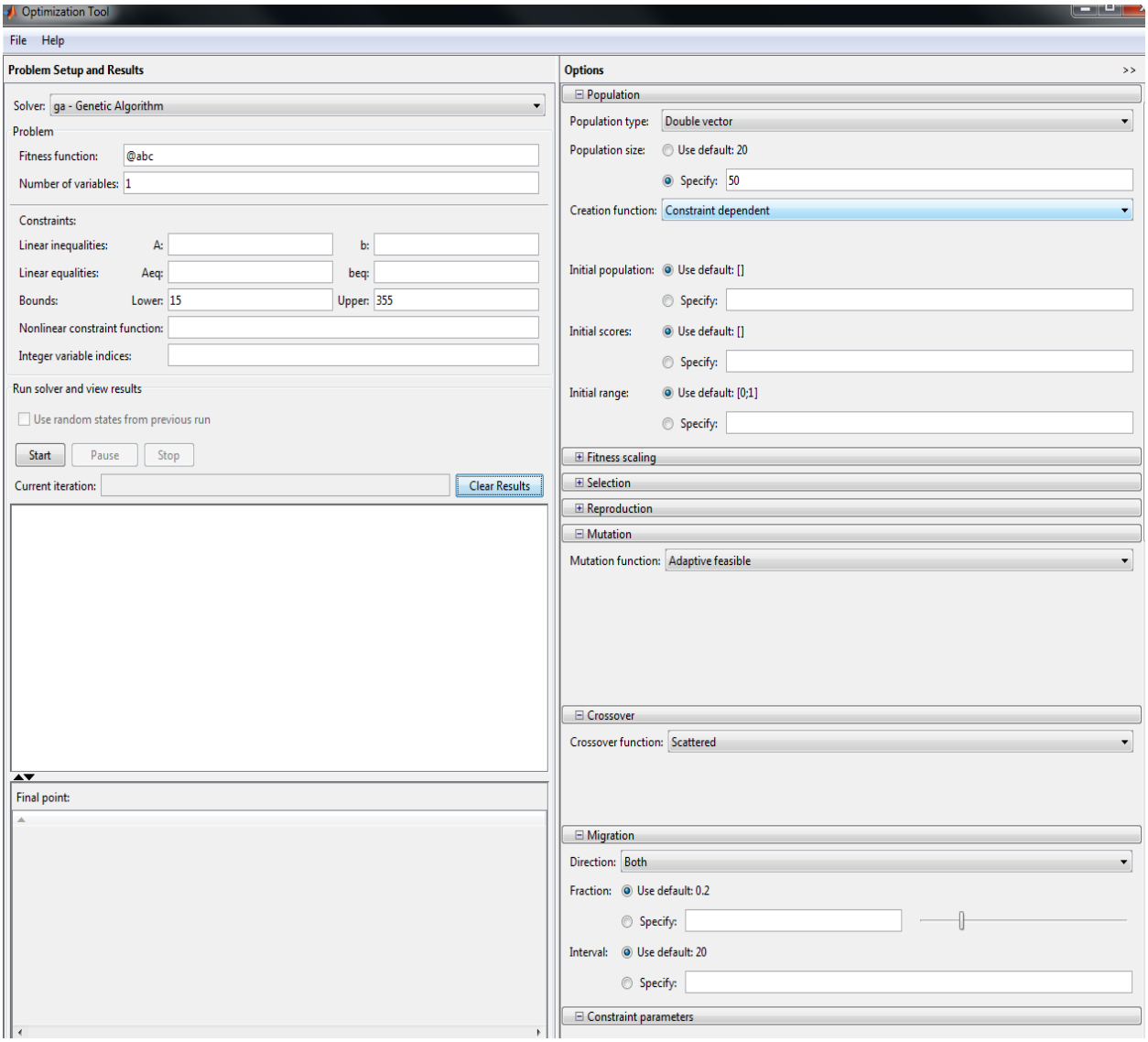

Figure 22: Genetic algorithm interface with population size 50, scattered crossover and both way migration

In this study, the following options of the GA algorithm were specified:

Option	*Parameter*	*Description*
Population		
Population type	Double vector	Individuals in the population

		have type *double*.
Population size	20, 50, 100	Specifies how many individuals there are in each generation. Large population size searches more thoroughly but takes more time.
Creation function	Constraint dependent	creates the initial population for ga.
Initial population	Default	specifies an initial population for the genetic algorithm
Initial score	Default	specifies initial scores for the initial population
Initial range	Default	specifies the range of the vectors in the initial population
Fitness Scaling		
Scaling function	Rank	scales the raw scores based on the rank of each individual instead of its score
Selection		
Selection Function	Stochastic uniform	The algorithm moves along the line in steps of equal size. At each step, the algorithm

		allocates a parent from the section it lands on
Reproduction	Default	specifies how the genetic algorithm creates children for the next generation
Mutation Function	Adaptive feasible	Randomly generates directions that are adaptive with respect to the last successful or unsuccessful generation. The mutation chooses a direction and step length that satisfies bounds and linear constraints.
Crossover	Scattered	specify how the genetic algorithm combines two individuals, or parents, to form a crossover child for the next generation
Stopping Criteria		
Stall generations	10	The algorithm stops if the average relative change in the best fitness function value over Stall generations is less than to the Function tolerance.

3.3 Analyzing temperature dependency of EIM parameters

To observe the variation of EIM parameters (i.e. resistance, reactance and phase) with respect to ambient temperature variation experimentally, a FEM model of human upper arm was developed using COMSOL Multiphysics 4.3a. The bicep girth measurement was 5 cm with constant 3 mm skin thickness. Simulation was done in a single frequency domain of 50 kHz and the inter electrode distance was fixed at 15mm-30mm-15mm formation. However, the effect of temperature variation in case of different stages of obesity was obtained by designing different models with varying skin-fat (SF) thickness. The values of conductivity and relative permittivity were obtained from previous studies. The equation that was solved for the potential measurement in this model is the Laplace equation:

$$\Delta . J_{Total} = \nabla . (\sigma . E + j\omega\varepsilon_0\varepsilon_r E) = 0 = \nabla . [(\sigma + j\omega\varepsilon_0\varepsilon_r) \nabla \phi] = 0 \quad (5)$$

Where J_{Total} is the current density, E is electric field, ϕ is potential and σ and ε are conductivity and permittivity respectively. A 1 mA test current was injected between the two current electrodes.

Temperature dependence of EIM parameters was obtained by performing a parametric sweep of temperature from 15^0C to 45^0C in the frequency domain study. The temperature dependency of biological tissues is similar to that of electrolyte solutions. Existing relationship between temperature and dielectric constants for electrolyte solutions as depicted in (6) and (7) was used in our study.

$$\sigma_T = \sigma_{To} (1 + \alpha (T - T_0)) \quad (6)$$

$$ln\varepsilon_r = A + BT + CT^2 \quad (7)$$

Where, σ_T = Conductivity at any temperature T°C, σ_{To} = Conductivity at calibration temperature T_0°C. α= temperature coefficient; ε_r =relative permittivity at any temperature T°C.

4 Results and Discussions

Rectangular shape of electrode is already accepted to find the EIM parameters using finite element model (FEM). As in EMG, circular electrodes are used to obtain the muscle electrical properties; my hypothesis was if it is possible to gain a better result using the same circular electrodes in EIM. For both of these electrodes the subcutaneous fat thickness was altered from 10mm to 24mm, which is a typical human fat thickness. As can be seen both for resistance and phase, there is a strong dependence on subcutaneous fat thickness across the frequency spectrum. But for both the electrode shapes, reactance appears to be less affected, demonstrating considerably smaller changes within the frequency range of interest (10 kHz to 100 kHz). In case of higher frequencies EIM parameters shows inconsistent behavior. Since as frequency increases, the current can begin to penetrate the sarcolemma and pass through the fibers directly (Martinsen 2011). At those higher frequencies, the proportion of intracellular free water may start to play a more important role. At low frequency, such as 10 kHz, both the electrode shapes provide almost same standard deviation. But in case of 100 kHz, the rectangular shape has a standard deviation of 2.04 ohm, where the circular shape has only 0.65 ohm. Also at higher frequencies, per mm increase of fat thickness in rectangular shape shows an increase of 0.5 ohm reactance, where the circular shows only 0.14 ohm. This provides the evidence of more efficiency of EIM with circular electrodes with the alteration of fat thickness.

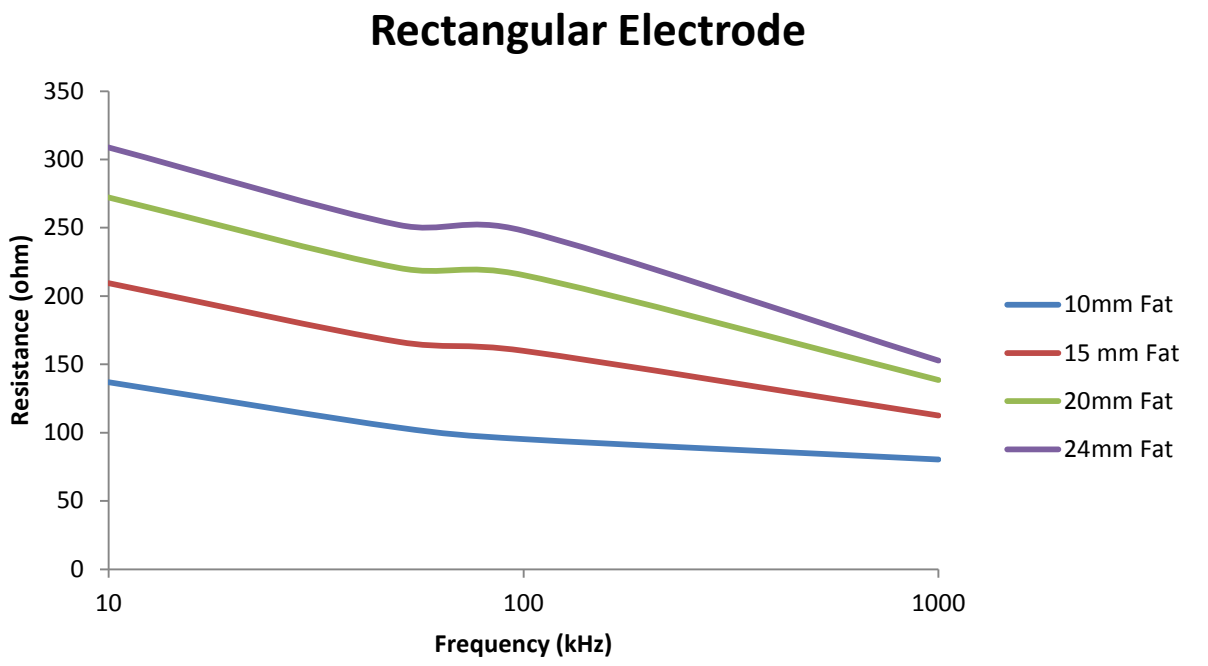
Rectangular Electrode
350
300
250
200
150
100
50
0
Resistance (ohm)
10
100
1000
Frequency (kHz)
10mm Fat
15 mm Fat
20mm Fat
24mm Fat

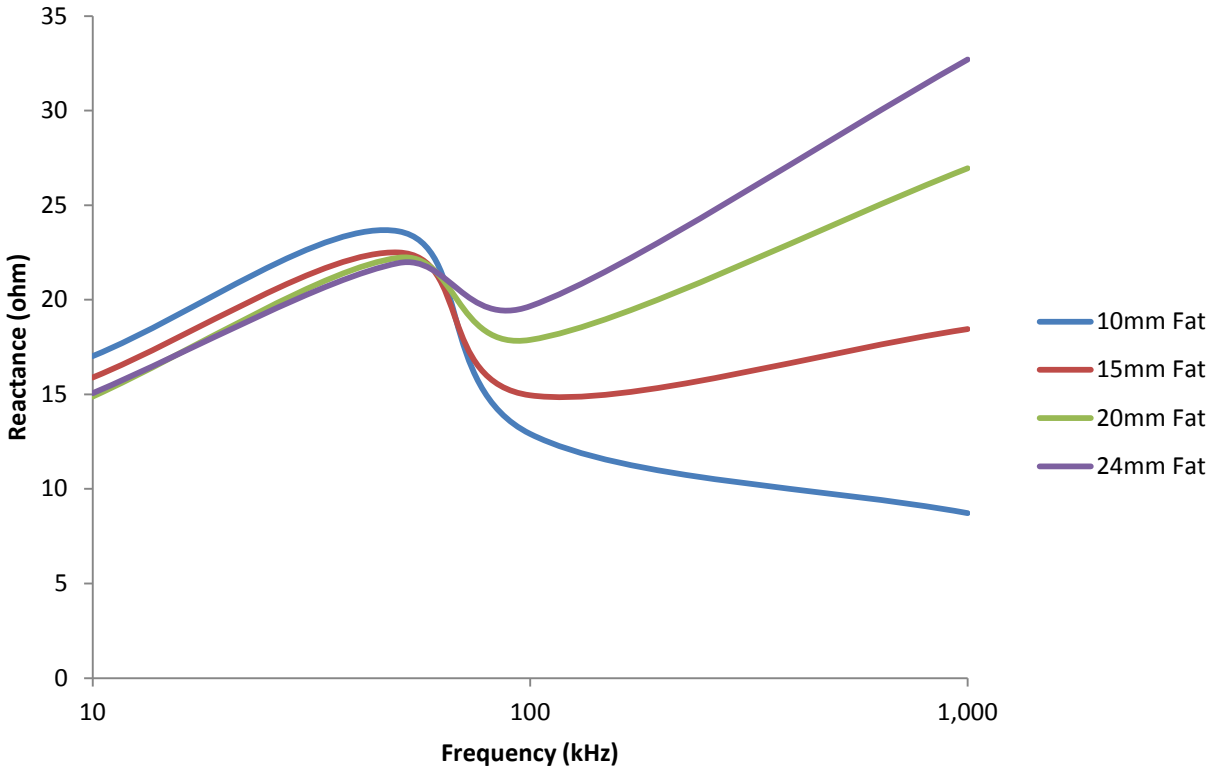
35
30
25
20
15
10
5
0
Reactance (ohm)
10
100
1,000
Frequency (kHz)
10mm Fat
15mm Fat
20mm Fat
24mm Fat

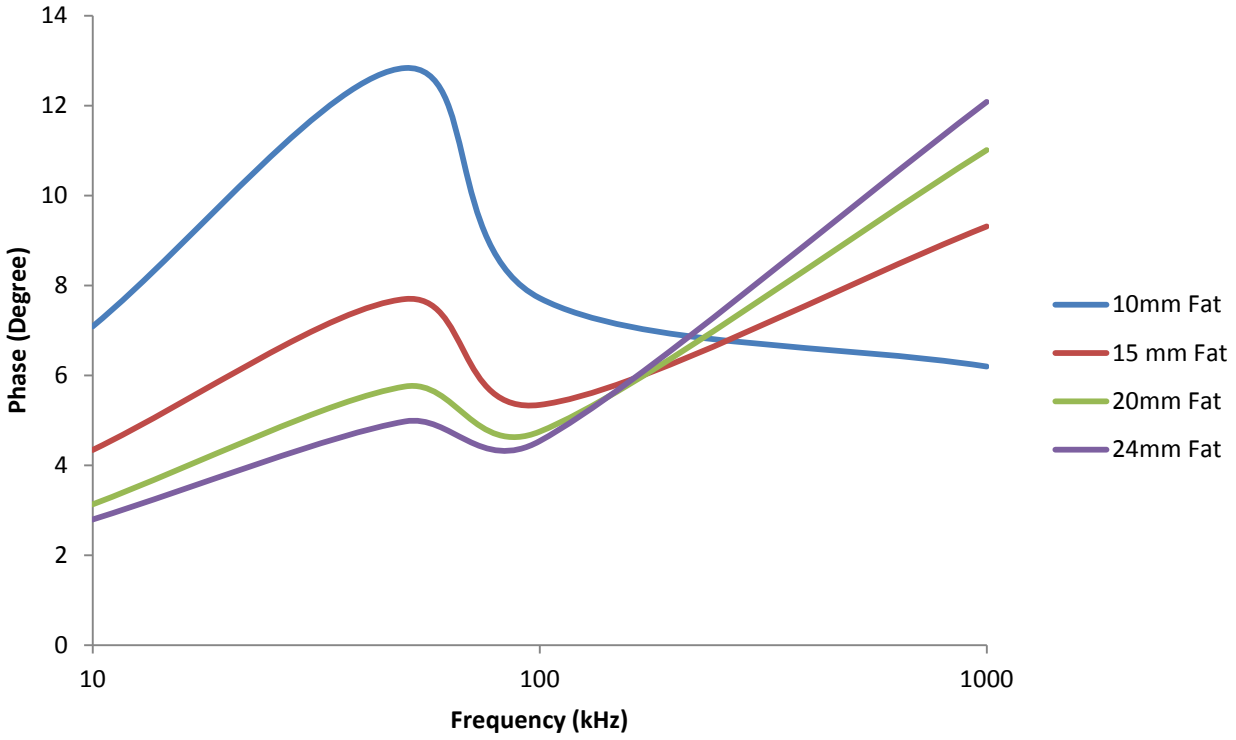

Figure 23: Resistance, reactance and phase obtained from FEM with rectangular shape of electrodes for different fat thickness

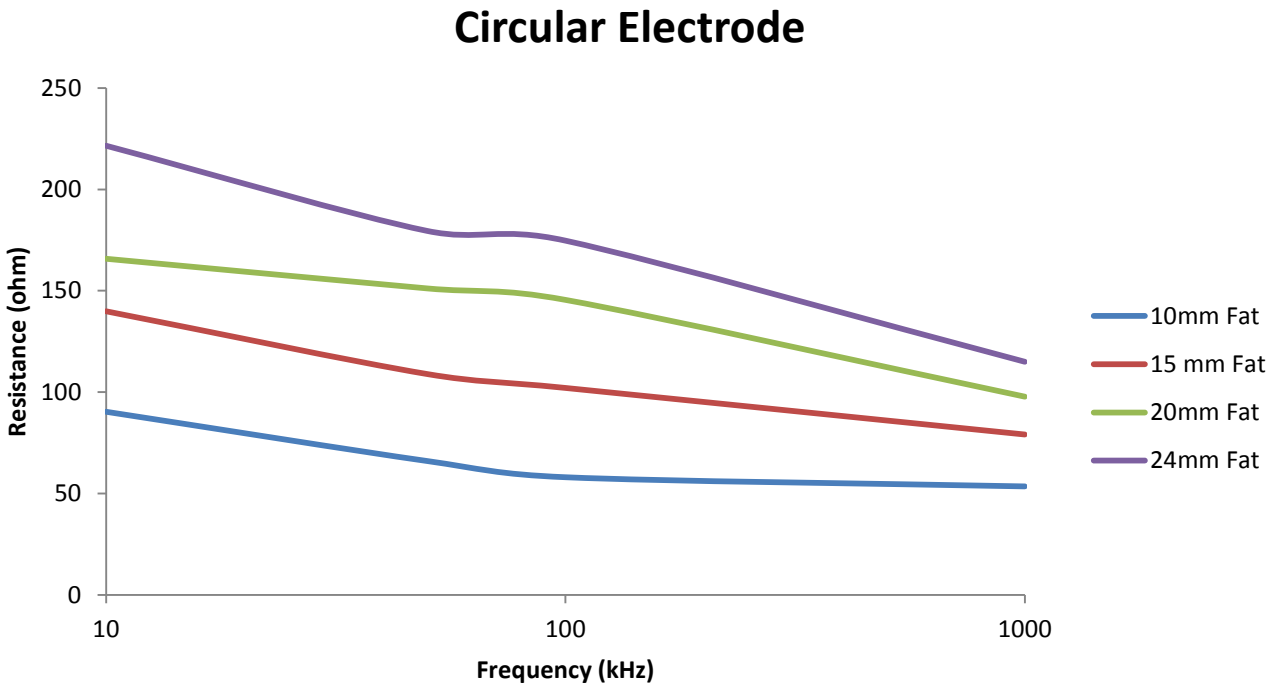

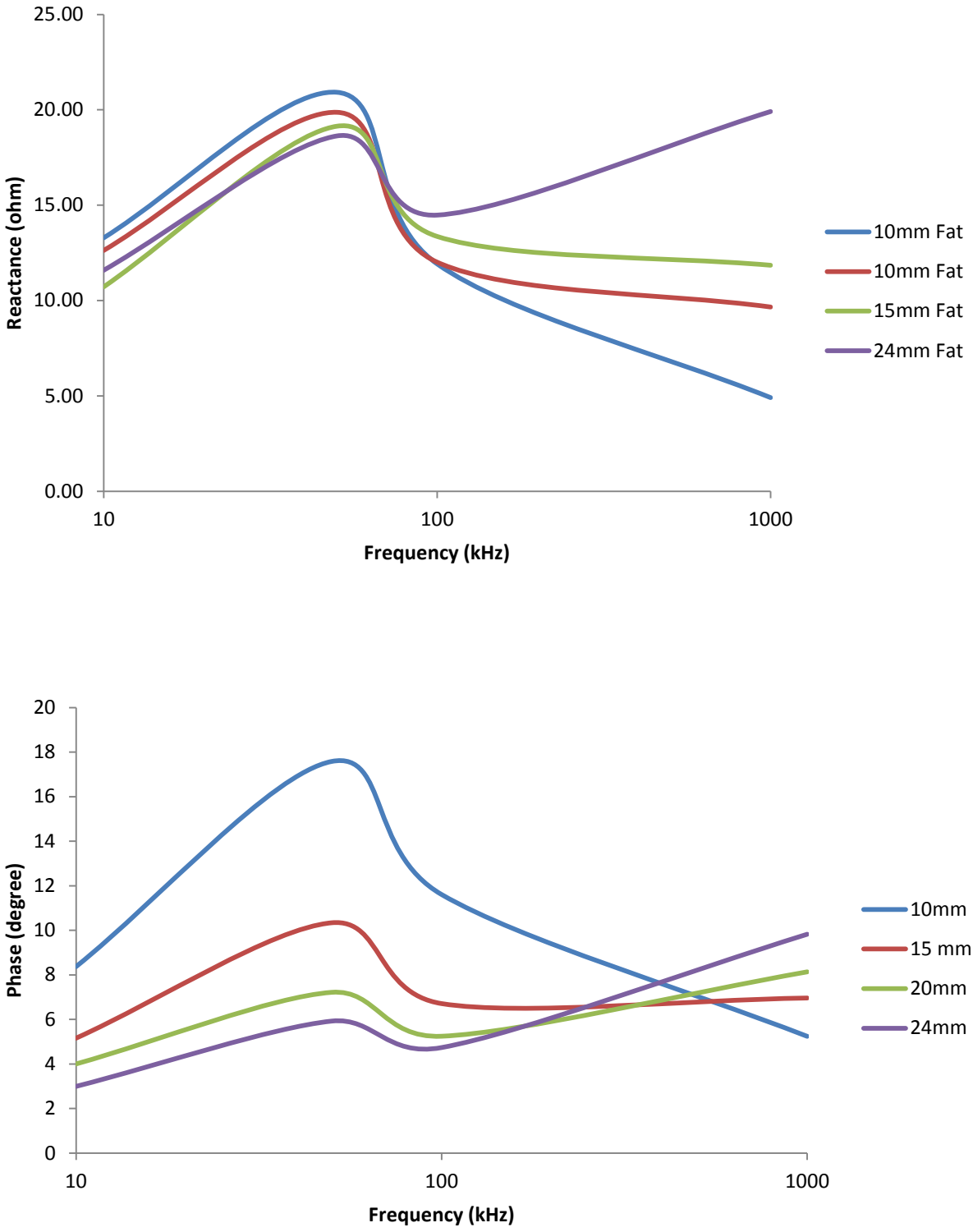

Figure 24: Resistance, reactance and phase obtained from FEM with circular shape of electrodes for different fat thickness

Now to further prove the FEM circular model as a neuromuscular disease diagnosis tool, it was simulated for acute crush and chronic crush conditions. In comparison to the normal condition, the acute crush and chronic crush condition demonstrate a flat profile of reactance. For all three scenarios, the maximum reactance value was obtained at 50 kHz frequency.

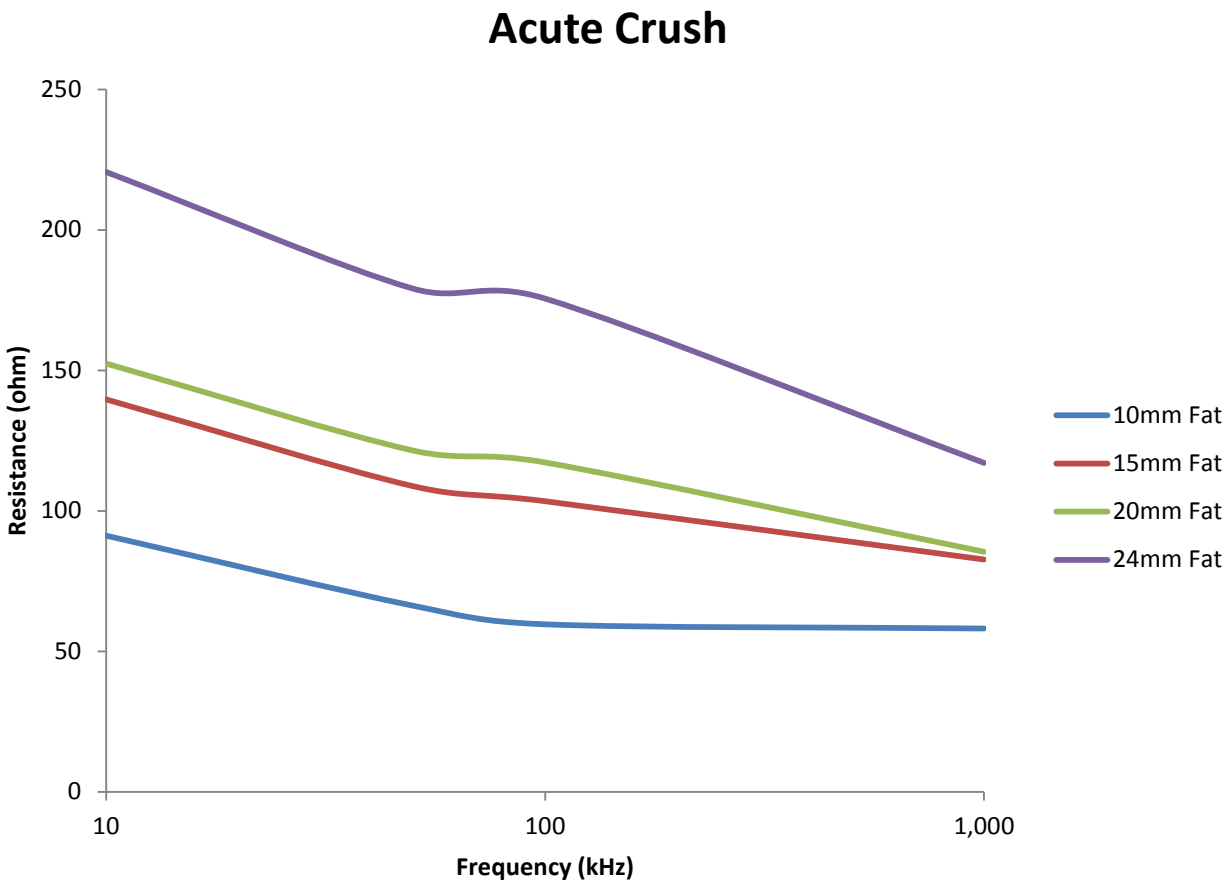

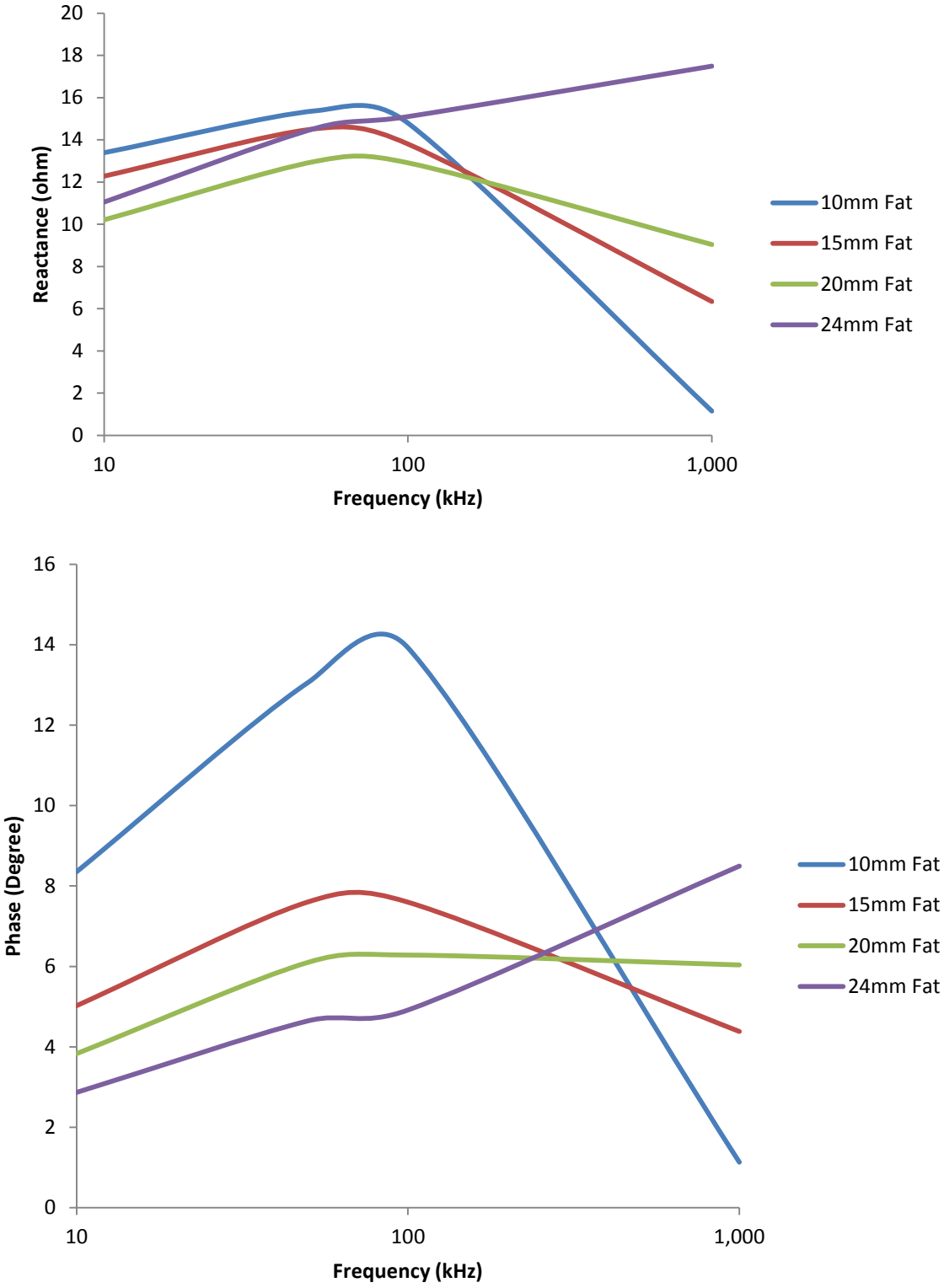

Figure 25: FEM predicted EIM properties in acute crush conditions

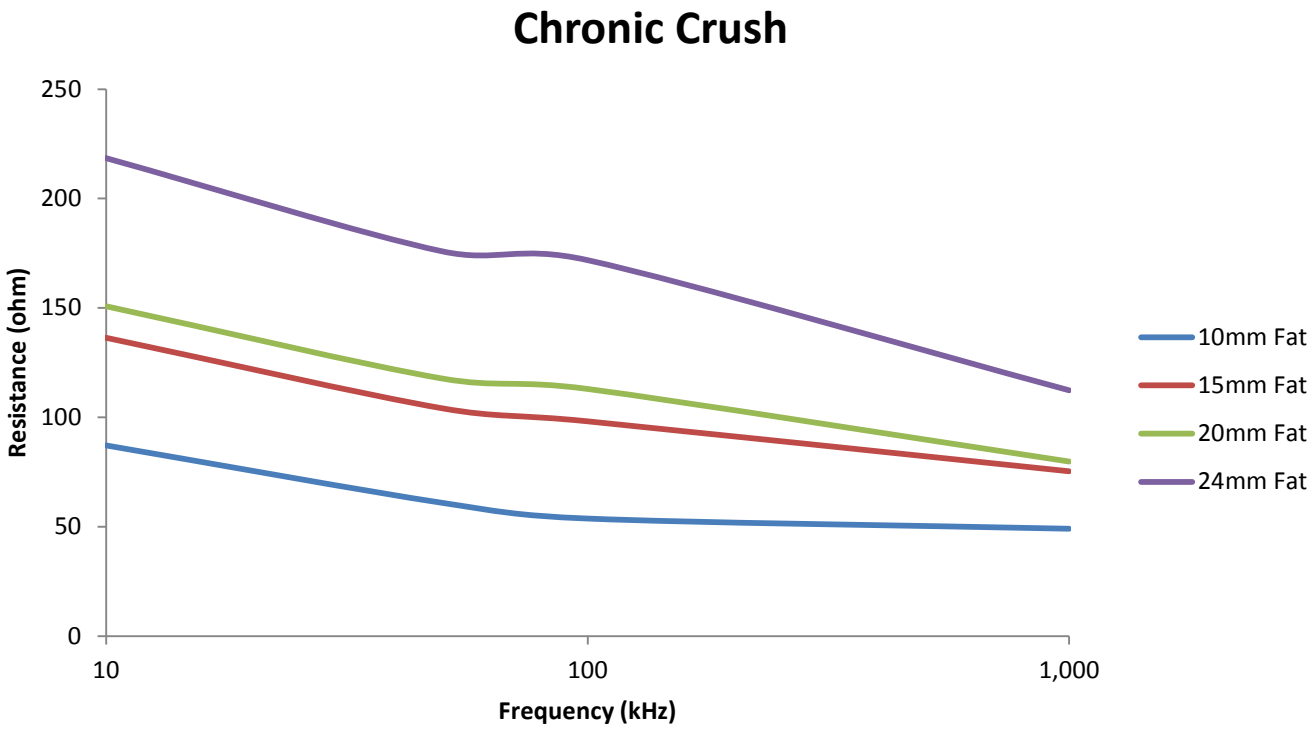
Chronic Crush
250
200
150
100
50
0
Resistance (ohm)
10
100
1,000
Frequency (kHz)
10mm Fat
15mm Fat
20mm Fat
24mm Fat

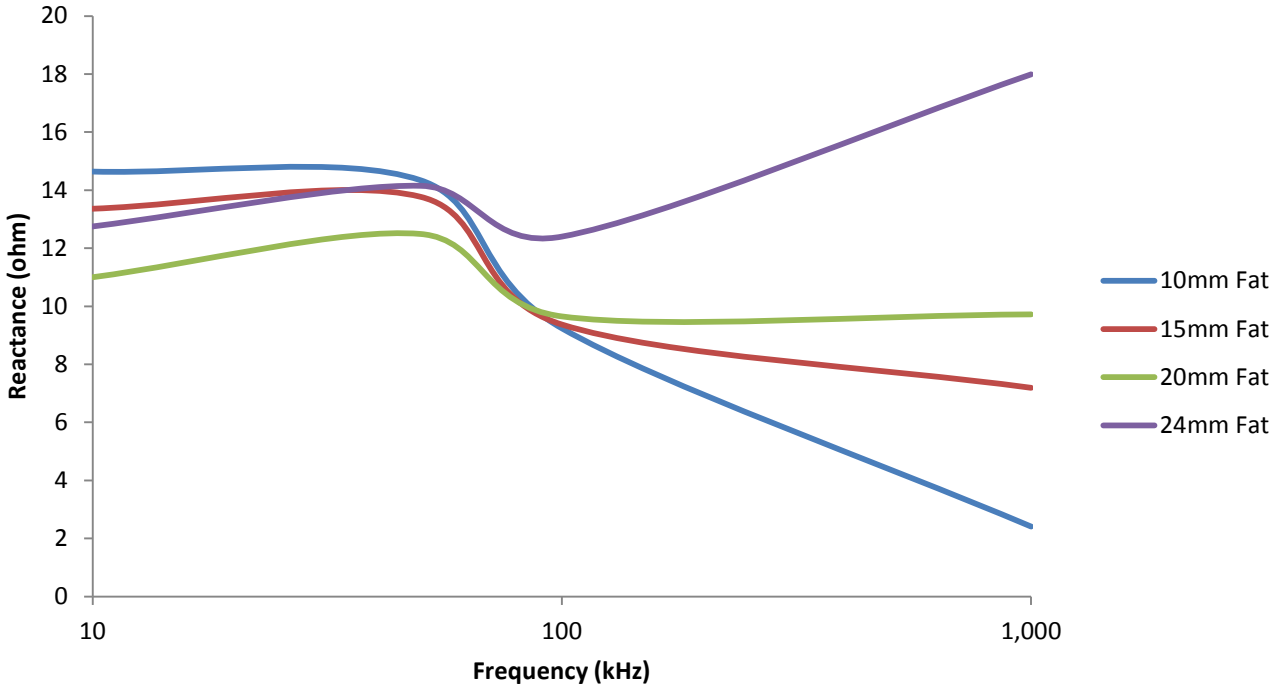
20
18
16
14
12
10
8
6
4
2
0
Reactance (ohm)
10
100
1,000
Frequency (kHz)
10mm Fat
15mm Fat
20mm Fat
24mm Fat

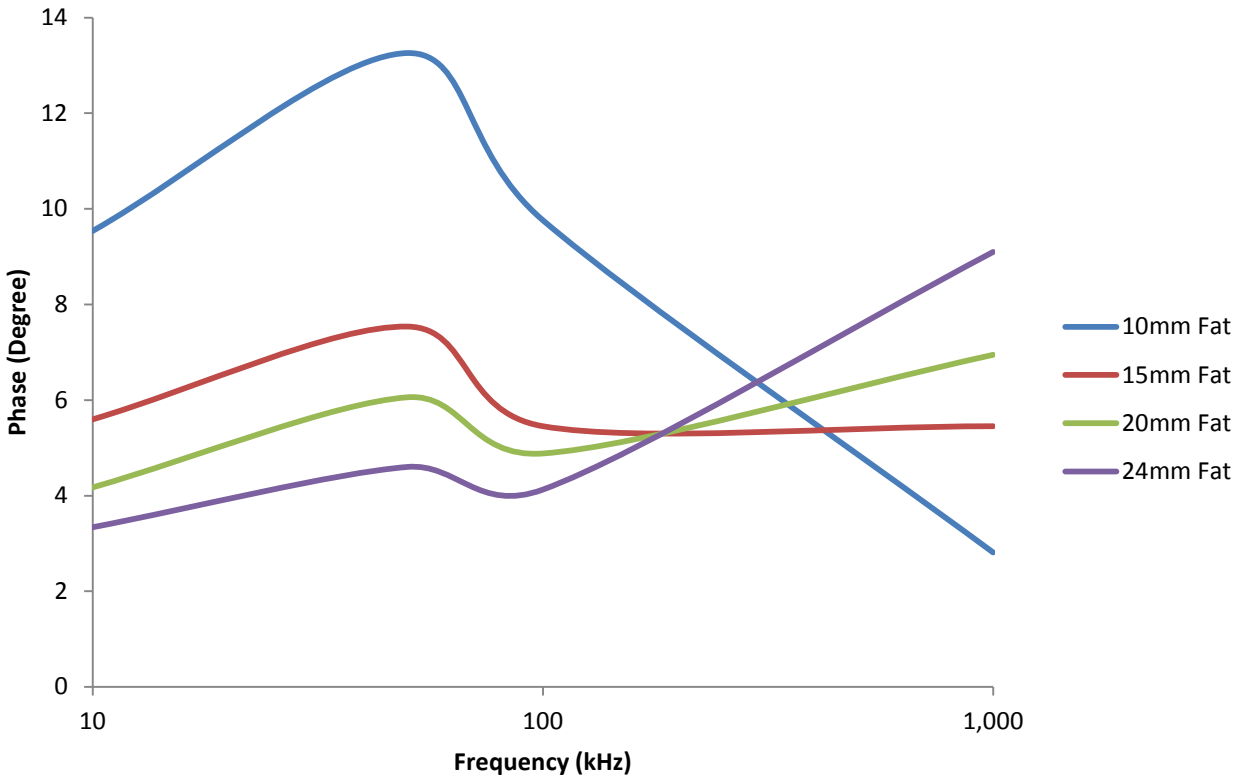

Figure 26: FEM predicted EIM properties in chronic crush conditions

Table 3: A comparison of the EIM parameters at 50 kHz frequency

EIM Parameter at 50 kHz	Normal	Acute	Chronic
Resistance (R) ohm	67	66	61
Reactance (X) ohm	21	13	14
Phase (P) degree	18	13	14

Also, with the 10mm baseline fat thickness, at normal condition reactance has a standard deviation of 3.96, where at acute crush and chronic crush condition, it is only 0.83 and 1.2 respectively. Thus the FEM model exhibits the confirmation of the proposed hypothesis.

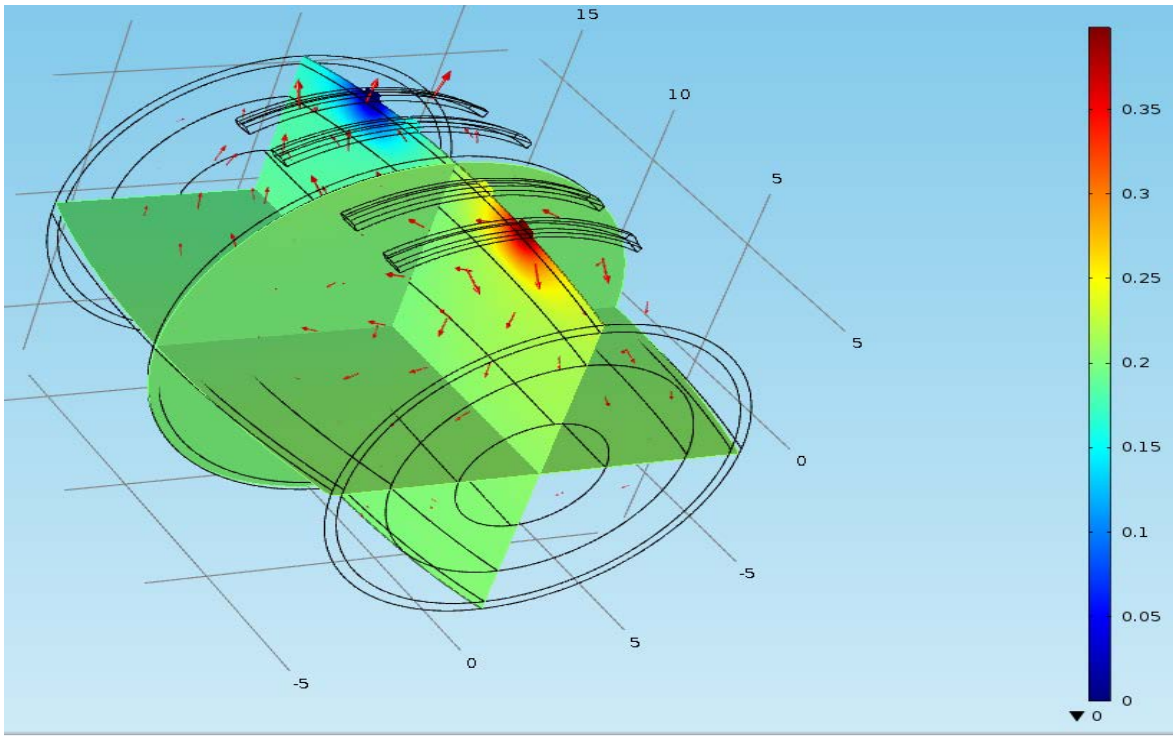

(a)

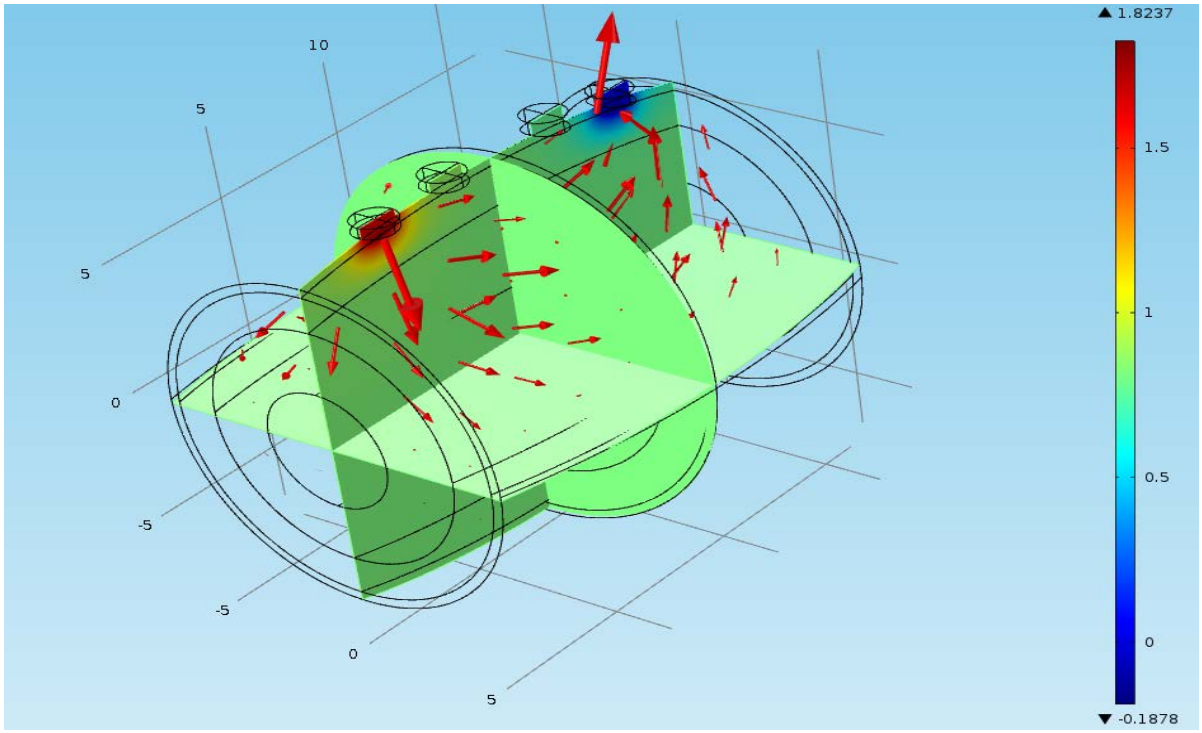

(b)

Figure 27: Comparison of current distribution (a) Rectangular electrodes (b) Circular electrodes

Performance with two different electrodes can be explained with the current distribution. Here the circumference of the rectangular and circular electrodes is 58 mm and 43.98 mm respectively. The rectangular electrodes cover larger portion than the circular electrodes. The electric field inside the bicep produces linear polarization for rectangular and elliptical polarization for circular electrodes. The reason behind that is for the circular electrodes maximum current passes through the skin and fat layer in perpendicular direction, which resulted in lower value of resistance. And the exact opposite phenomenon resulted in higher value of resistance for rectangular electrodes. The advantage of using the circular electrode is more current can pass through the fat layer to the muscle layer even though the fat thickness is increased. The impact on muscle due to current injection is very low for rectangular shape of electrodes when the fat thickness is high.

In this study, genetic algorithm was run for three different population sizes. The purpose of the ga algorithm was to find the angle of rotation of the electrodes for which the percentage change in reactance is minimal with two different fat thicknesses of 5mm and 15mm. the following table shows the ga algorithm output for different population sizes:

Table 4: Output for different population sizes

Population Size	Resulted angle of rotation of the electrodes (degree)
20	323.49^0
60	72.13^0
75	70.19^0
100	71.48^0

With a small population size, the ga algorithm chose a small value for the individuals for each generation. Thereby, it missed some portion of the solution space. So the resulted angle with 20 population size was for the local minimum of the percentage change of reactance, not the global minimum. But with the higher values of population size, the resulted angles were very close. But with population size more than 60, caused the algorithm to run very slowly. So, the optimal population size considered in the ga algorithm was 60.

All of the three major EIM parameters (i.e. resistance, reactance and phase) were found to be having a downward slope with temperature increment. The temperature sweep was performed from 10^{o}C to 45^{o}C. A sample variation of EIM parameters with 20mm subcutaneous fat (SF) thickness is illustrated in Figure 30. It was found during our studies that, in case of larger cross sectional area of SF thickness the percentage change in resistance with respect to temperature increases while the percentage change in reactance decreases with SF thickness increment as listed in Table 5.

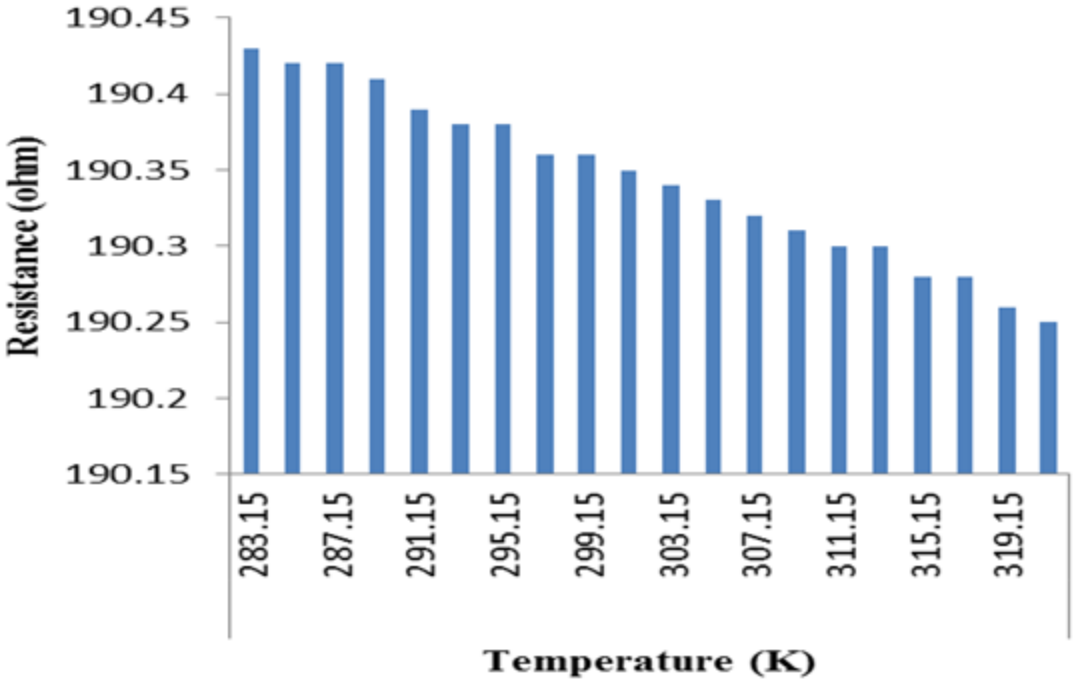
190.45
190.4
190.35
190.3
190.25
190.2
190.15
Resistance (ohm)
283.15
287.15
291.15
295.15
299.15
303.15
307.15
311.15
315.15
319.15
Temperature (K)

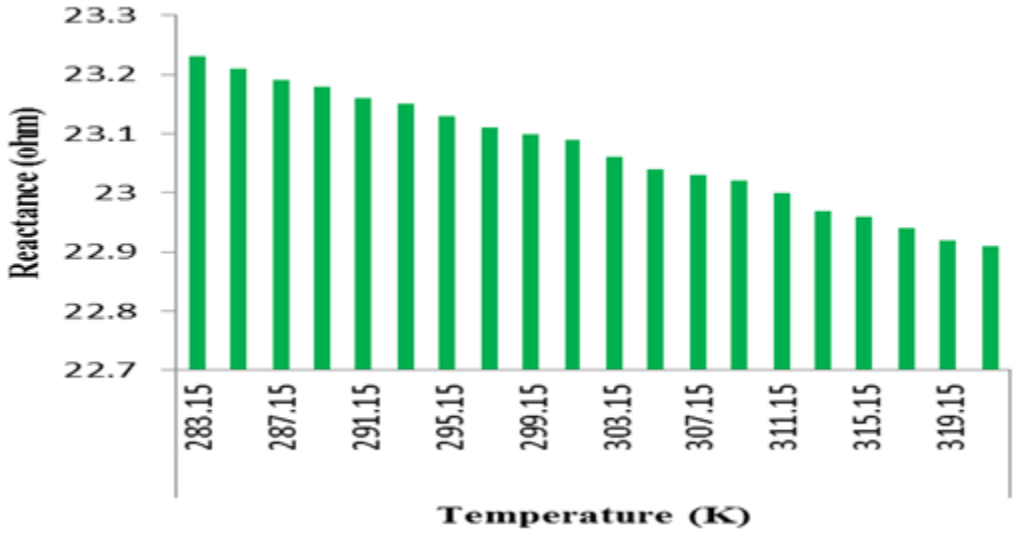
23.3
23.2
23.1
23
22.9
22.8
22.7
Reactance (ohm)
283.15
287.15
291.15
295.15
299.15
303.15
307.15
311.15
315.15
319.15
Temperature (K)

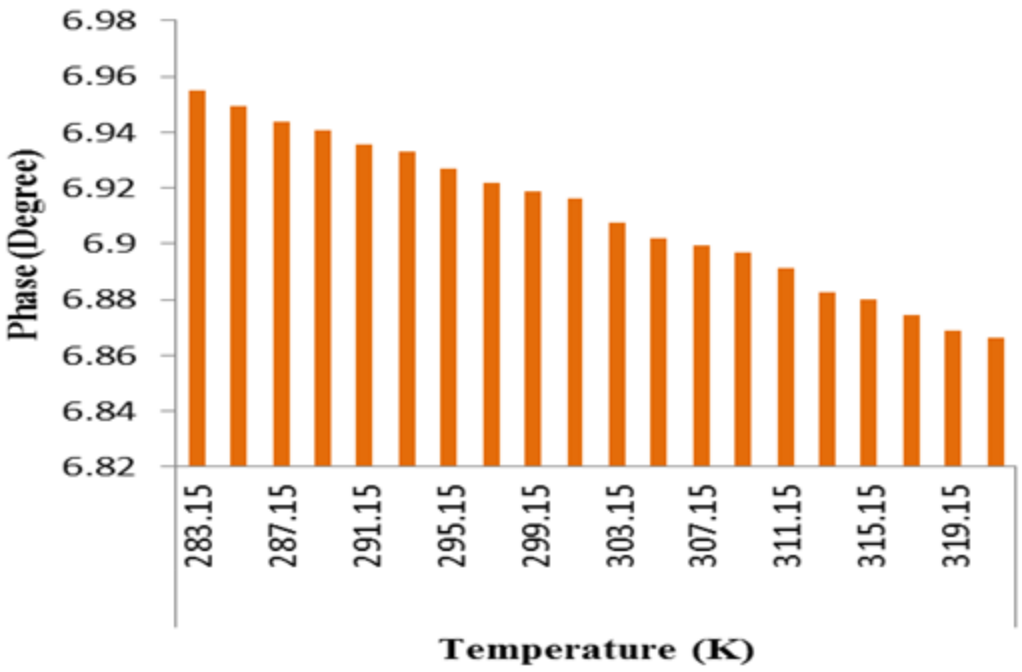

Figure 28: Variation of a) Resistance b) Reactance c) Phase with respect to the ambient temperature (simulated within the range 10-45 degree Celsius)

Table 5: EIM parameters percentage deviation per °celsius

Fat(mm)	*% Change in R*	*% Change in X*	*% Change in Phase*
10	0.32%	1.50%	1.01%
15	0.42%	1.39%	0.56%
20	0.47%	0.84%	0.23%
24	0.53%	0.29%	0.06%

The variation in EIM parameters with temperature can easily be explained by exploring the effect of temperature on electrolyte solution. Increasing temperature causes the viscosity of a solvent to decrease. In turn, ion mobility increases, also causing conductivity to increase. In case of higher SF thickness, the current distribution has to pass through a larger cross sectional area of region with much less conductivity, hence the resistance increases. On the other hand, change in reactance with varying fat thickness is quite negligible in comparison to resistance. Physically, in case of larger SF thickness increasing temperature causes the capacitance formed between different layers of body tissue to decrease in a slower rate. That's why; the temperature dependency of reactance is quite opposite to the relationship between resistance and temperature. The finding of this study implies that there is a very small and negligible change in EIM parameters for different geographical conditions and hence the effect of temperature on EIM parameters can be ignored to some extent. This study is the basis for our future EIM modeling for temperature dependence in which effects of temperature difference between inside and outside of the muscle EIM model will be analyzed.

5 Conclusion and Scope of Future Work

In this study, different approaches were conducted to find the least dependency of EIM parameters resistance, reactance and phase due to change in subcutaneous fat thickness. As rectangular shape of electrodes was already accepted as a measuring tool to find the EIM parameters using finite element model (FEM), in this study the FEM model was designed for both rectangular and proposed circular shape of electrodes. Several important observations were made during the modeling of the human upper arm. EIM parameter resistance depends on the dielectric properties of the skin and fat layer. Dependency of reactance on the skin and fat layer dielectric properties is very negligible. But, EIM parameter reactance depends on the anisotropic dielectric properties of the muscle layer, muscle layer properties has very little effects on the resistance value. As EIM is a neuromuscular disease diagnosis tool, reactance is considered as most suitable parameters among three.

The major challenge with the rectangular shape of electrode is that it has significant dependency on subcutaneous fat thickness. From the current distribution of the rectangular shape, it was observed that from the current injecting source electric field does not passes in perpendicular direction, rather it passes in a diagonal direction. Due to diagonal direction, the horizontal component of it passes through the isotropic skin and fat layer, and the vertical component passes through the skin, fat and muscle layer. In the skin and fat layer current can only flow in vertical direction due to their isotropic property, so the horizontal component of the electric field get nullified, resulted in higher resistance. But in case of circular electrode, from the current injecting source, the horizontal component of the electric field is very minimum, most of the electric field passes in vertical direction in skin, fat and muscle layer. As the horizontal

component of the electric field does not contribute to the resistance anymore, it resulted in less resistance.

It is mentioned earlier that reactance highly depends on the dielectric properties of the muscle layer. For rectangular shape of electrodes, a significant portion of the electric field passes through horizontal direction, so with the increment of fat thickness, current density inside the muscle decreases. But in case of circular electrode, most of the electric field passes through all the layers in vertical direction. So with the increase in fat thickness, current distribution inside the muscle does not change significantly for circular electrodes.

In order to seek out an optimized shape other than rectangular or circular shape which is least effected by SF thickness alteration, in this study genetic algorithm is also proposed. The only variable used for the algorithm is the angle of rotation of the electrode with respect to the perpendicular axis. Though the algorithm is performed for different population size, the best result of 72^0 is obtained for a population size of 60.

Area, axis of revolution, muscle thickness, inter-electrode distance etc. can be other vital parameter for modeling the optimized electrode shape. Considering these new variables brings in many new challenges. Such as, the new optimized electrodes might penetrate into skin, fat or muscle layer and can also result in some unconventional shapes, which is not desirable. To verify the finite element model and genetic algorithm result, EIM experiment can be performed on large number of people. In future, using ultrasound, fat and muscle thickness can be measured and incorporated in the FEM model.

Electrical impedance myography (EIM) can quantify the status of the underlying muscle tissue and thus, noninvasively obtain new information about the status of diseased muscle in human

subjects. Further refinement of electrode configurations is needed to optimize EIM for clinical use; this can be achieved with further modeling and detailed study on human subjects.

Reference

Ahad, Mohammad A., and and Seward B. Rutkove. "Electrical Impedance Myography at 50 kHz in the rat technique, reproducibility, and the effects of sciatic injury and recovery." *Clinical Neurophysiology*, 2009: 1534-1538.

Ahad, Mohammad A., P. Michelle Fogerson, Glenn D. Rosen, Pushpa Narayanaswami, and and Seward B. Rutkove. "Ahad, Mohammad A., P. Michelle Fogerson, Glenn D. Rosen, Pushpa Narayanaswami, andElectrical characteristics of rat skeletal muscle in immaturity, adulthood and after sciatic nerve injury, and their relation to muscle fiber size." *Physiological Measurements*, 2009: 1415.

Esper, Gregory J., Carl A. Shiffman, Ronald Aaron, Kyungmouk S. Lee, and and Seward B. Rutkove. "Esper, Gregory J., Carl A. Shiffman, Ronald Aaron, Kyungmouk S. Lee, andAssessing neuromuscular disease with multifrequency electrical impedance myography." *Muscle & Nerve Volume 34, Issue 5*, 2006: 595-602.

Garmirian, Lindsay P., Anne B. Chin, and and Seward B. Rutkove. "Garmirian, Lindsay P., Anne B. Chin,Discriminating neurogenic from myopathic disease via measurement of muscle anisotropy." *Muscle & Nerve*, 2009: 16-24.

Hardyck, C, L Petrincovich, and D Ellsworth. "Feedback of Speech Muscle Activity During Silent Reading: Rapid Extension." *Science*, 1966: 154.

Jafarpoor, Mina, Jia Li, J. White, and and S. Rutkove. "Jafarpoor, Mina, Jia Li, J. WhOptimizing electrode configuration for electrical impedance measurements of muscle via the finite element method." *Biomedial Engineering, IEEE transactions*, 2013: 1446-1452.

Kaplanis, P. A., et al. "Surface EMG analysis on normal subjects based on isometric voluntary contraction." *Journal of Electromyography and Kinesiology*, 2009: 157-171.

Martinsen, Orjan G., and Sverre Grimnes. *Bioimpedance and bioelectricity basics.* London: Academic Press, 2011.

Narayanaswami, Pushpa, Andrew J. Spieker, Phillip Mongiovi, John C. Keel, Stefan C. Muzin, and and Seward B. Rutkove. "Narayanaswami, Pushpa, Andrew J. Spieker, Phillip Mongiovi, John C. Utilizing a handheld electrode array for localized muscle impedance measurements." *Muscle & Nerve,* 2012: 257-263.

nysora.com. n.d.

Peetrons, P. "Ultrasound of muscles." *European radiology 12.1*, 2002: 35-43.

Pillen, Sigrid, Ilse MP Arts, and Machiel J. Zwarts. "Muscle ultrasound in neuromuscular disorders." *Muscle & Nerve,* 2008: 679-693.

Rutkove, Seward B. "Electrical impedance myography: background, current state, and future directions." *Muscle & Nerve,* 2009: 936-946.

Rutkove, Seward B., et al. "Electrical impedance myography to assess outcome in amyotrophic lateral sclerosis clinical trials." *Clinical Neurophysiology Volume 128, Issue 11*, 2007: 2413-2418.

Shiffman, C, R. Aaron, and A. Altman. "Spatial dependence of the phase in localized bioelectrical impedance analysis." *Muscle & Nerve,* 2002: 390.

Sung, Minhee, Andrew J. Spieker, Pushpa Narayanaswami, and and Seward B. Rutkove. "Sung, Minhee, Andrew J. Spieker, Pushpa Narayanaswami, and SewarThe effect of subcutaneous fat on electrical impedance myography when using a handheld electrode array: The case for measuring reactance." *Clinical Neurophysiology, volume 124, issue 2,* 2013: 400-404.

Wang, Lucy L., Mohammad Ahad, Alistair McEwan, Jia Li, Mina Jafarpoor, and and Seward B. Rutkove. "Wang, Lucy L., Mohammad Ahad, Alistair McEwan, Jia Li, Mina Jafarpoor, and SAssessment of alterations in the electrical impedance of muscle after experimental nerve injury via finite-element analysis." *Biomedical Engineering, IEEE Transactions on (Volume:58 , Issue: 6)* , 2011: 1585-1591.

Appendix A

Standard Deviation

A measure of the dispersion of a set of data from its mean. The more spread apart the data, the higher the deviation. Standard deviation is calculated as the square root of variance. The equation to calculate the standard deviation is:

$$\sigma = \sqrt{\frac{1}{N}\sum(X_i - \mu)^2}$$

Here, μ = mean of the samples,

x_i = Each value of the sample,

N =Sample Size,

σ = Standard Deviation.

T test:

A t-test asks whether a difference between two groups' averages is unlikely to have occurred because of random chance in sample selection. A difference is more likely to be meaningful if

(1) the difference between the averages is large,

(2) the sample size is large, and

(3) responses are consistently close to the average values and not widely spread out (the standard deviation is low).

The t-test's statistical significance and the t-test's effect size are the two primary outputs of the t-test. Statistical significance indicates whether the difference between sample averages is likely to

represent an actual difference between populations (as in the example above), and the effect size indicates whether that difference is large enough to be practically meaningful.

The **"One Sample T-Test"** is similar to the "Independent Samples T-Test" except it is used to compare one group's average value to a single number (for example, do Kansans on average spend more than $13 per month on movies?). For practical purposes you can look at the confidence interval around the average value to gain this same information.

The **"paired t-test"** is used when each observation in one group is paired with a related observation in the other group. For example, do Kansans spend more money on movies in January or in February, where each respondent is asked about their January and their February spending? In effect a paired t-test subtracts each respondent's January spending from their February spending (yielding the increase in spending), then take the average of all those increases in spending and looks to see whether that average is statistically significantly greater than zero (using a one sample t-test).

The "***ranked*** **independent samples t-test**" asks a similar question to the typical *unranked* test but it is more robust to outliers (a few bad outliers can make the results of an unranked t-test invalid).

Appendix B

Matlab code for the design of human upper arm

```
function [pot1,pot2] = model_fn(SFat,BCrntSrc,angl1,angl2)
close all;
import com.comsol.model.*
import com.comsol.model.util.*

model = ModelUtil.create('Model');
model.geom.create('geom1', 3);
model.physics.create('ec', 'ConductiveMedia', 'geom1');
model.geom('geom1').lengthUnit('cm');
model.geom('geom1').feature.create('hel1', 'Helix');
model.geom('geom1').feature('hel1').set('turns', '1.1');
model.geom('geom1').feature('hel1').set('rmaj', '.1');
model.geom('geom1').feature('hel1').set('rmin', '2.15');
model.geom('geom1').feature('hel1').set('axialpitch', '15');
model.geom('geom1').feature('hel1').setIndex('ax3', '1', 0);
model.geom('geom1').feature('hel1').setIndex('ax3', '-.03', 1);
model.geom('geom1').feature('hel1').setIndex('ax3', '0', 2);
model.geom('geom1').feature('hel1').set('endcaps', 'perpspine');
model.geom('geom1').feature.create('elp1', 'Ellipsoid');
model.geom('geom1').feature('elp1').setIndex('semiaxes', '5.075', 0);
model.geom('geom1').feature('elp1').setIndex('semiaxes', '5.12', 1);
model.geom('geom1').feature('elp1').setIndex('semiaxes', '15.5', 2);
model.geom('geom1').feature('elp1').setIndex('pos', '8.3', 0);
model.geom('geom1').feature('elp1').setIndex('pos', '-.1', 1);
model.geom('geom1').feature('elp1').setIndex('pos', '.1', 2);
model.geom('geom1').feature('elp1').setIndex('ax3', '1', 0);
model.geom('geom1').feature('elp1').setIndex('ax3', '-.04', 1);
model.geom('geom1').feature('elp1').setIndex('ax3', '0', 2);
model.geom('geom1').feature.copy('elp2', 'geom1/elp1');
model.geom('geom1').feature('elp2').setIndex('semiaxes', 5.075+SFat, 0);
model.geom('geom1').feature('elp2').setIndex('semiaxes', 5.12+SFat, 1);
model.geom('geom1').feature('elp2').setIndex('semiaxes', '16', 2);
model.geom('geom1').feature.copy('elp3', 'geom1/elp1');
model.geom('geom1').feature('elp3').setIndex('semiaxes', 5.075+SFat+0.3, 0);
model.geom('geom1').feature('elp3').setIndex('semiaxes', 5.12+SFat+0.3, 1);
model.geom('geom1').feature('elp3').setIndex('semiaxes', '16.5', 2);
model.geom('geom1').feature.create('cyl1', 'Cylinder');
model.geom('geom1').feature('cyl1').set('r', '9');
model.geom('geom1').feature('cyl1').set('h', '25');
model.geom('geom1').feature('cyl1').setIndex('pos', '-24.9', 0);
model.geom('geom1').feature('cyl1').setIndex('ax3', '1', 0);
model.geom('geom1').feature('cyl1').setIndex('ax3', '0', 2);
model.geom('geom1').feature.create('dif1', 'Difference');
model.geom('geom1').feature('dif1').selection('input').set({'elp1' 'elp2'
'elp3' 'hel1'});
model.geom('geom1').feature('dif1').selection('input2').set({'cyl1'});
model.geom('geom1').feature.create('cyl2', 'Cylinder');
model.geom('geom1').feature('cyl2').set('r', '9');
model.geom('geom1').feature('cyl2').set('h', '25');
model.geom('geom1').feature('cyl2').setIndex('pos', '16.3', 0);
model.geom('geom1').feature('cyl2').setIndex('ax3', '1', 0);
```

```
model.geom('geom1').feature('cyl2').setIndex('ax3', '0', 2);
model.geom('geom1').feature.create('dif2', 'Difference');
model.geom('geom1').feature('dif2').selection('input').set({'dif1'});
model.geom('geom1').feature('dif2').selection('input2').set({'cyl2'});


poly1=[5.12+SFat-.22,5.12+SFat-.12,5.12+SFat+.48,5.12+SFat+.48,5.12+SFat-
.22];
poly2=[5.12+SFat-.02,5.12+SFat+.08,5.12+SFat+.53,5.12+SFat+.53,5.12+SFat-
.02];


model.geom('geom1').feature.create('wp1', 'WorkPlane');
model.geom('geom1').feature('wp1').geom.feature.create('pol1', 'Polygon');
model.geom('geom1').feature('wp1').geom.feature('pol1').set('x',
'2.757,3.457,3.457,2.757,2.757');
model.geom('geom1').feature('wp1').geom.feature('pol1').set('y', poly1);
model.geom('geom1').feature('wp1').geom.feature.create('pol2', 'Polygon');
model.geom('geom1').feature('wp1').geom.feature('pol2').set('x',
'5.657,6.357,6.357,5.657,5.657');
model.geom('geom1').feature('wp1').geom.feature('pol2').set('y', poly2);
model.geom('geom1').feature.create('rev1', 'Revolve');
model.geom('geom1').feature('rev1').selection('input').set({'wp1.pol1'});
model.geom('geom1').feature('rev1').setIndex('pos', '3.457', 0);
model.geom('geom1').feature('rev1').setIndex('pos', poly1(3), 1);
model.geom('geom1').feature('rev1').setIndex('axis', '-.2', 1);
model.geom('geom1').feature('rev1').set('angle1', angl1);   %starting
revolution angle for current electrode
model.geom('geom1').feature('rev1').set('angle2', angl2);   %ending
revolution angle for current electrode
model.geom('geom1').feature.copy('rev2', 'geom1/rev1');
model.geom('geom1').feature('rev2').selection('input').set({'wp1.pol2'});
model.geom('geom1').feature('rev2').setIndex('pos', '6.357', 0);
model.geom('geom1').feature('rev2').setIndex('pos', poly2(3), 1);
model.geom('geom1').feature('rev2').set('angle1', angl1);   %starting
revolution angle for sense electrode
model.geom('geom1').feature('rev2').set('angle2', angl2);    %ending
revolution angle for sense electrode


model.geom('geom1').feature.create('mir1', 'Mirror');
model.geom('geom1').feature('mir1').selection('input').set({'rev1' 'rev2'});
model.geom('geom1').feature('mir1').setIndex('pos', '8.557', 0);
model.geom('geom1').feature('mir1').setIndex('pos', 5.12+SFat+0.3, 1);
model.geom('geom1').feature('mir1').setIndex('pos', '.1', 2);
model.geom('geom1').feature('mir1').setIndex('axis', '1', 0);
model.geom('geom1').feature('mir1').setIndex('axis', '-.04', 1);
model.geom('geom1').feature('mir1').setIndex('axis', '0', 2);
model.geom('geom1').feature('mir1').set('keep', 'on');

model.geom('geom1').feature.create('dif3', 'Difference');
model.geom('geom1').feature('dif3').selection('input').set({'mir1' 'rev1'
'rev2'});
model.geom('geom1').feature('dif3').selection('input2').set({'dif2'});
model.geom('geom1').feature('dif3').set('keep', 'on');
```

```
model.geom('geom1').run;


model.geom('geom1').feature.create('del1', 'Delete');
model.geom('geom1').feature('del1').selection('input').init(3);
model.geom('geom1').feature('del1').selection('input').set('rev1',1);
model.geom('geom1').feature('del1').selection('input').set('rev2',1);
model.geom('geom1').feature('del1').selection('input').set('mir1(2)',1);
model.geom('geom1').feature('del1').selection('input').set('mir1(1)',1);
% model.geom('geom1').run('fin');
model.geom('geom1').run;

%% Finding the face for boundary current source
upDown = model.geom('geom1').getUpDown;
upDown = int32(upDown');
domain = cell(1,length(upDown));
for i = 1:length(domain)
domain{upDown(i,2)} = cat(2,domain{upDown(i,2)},i);
end
u=cell2mat(domain(5));
v=cell2mat(domain(8));
a=u(1):1:u(length(u));
b=v(1):1:v(length(v));
crntFace=setdiff(a,u);
grndFace=setdiff(b,v);

            %%%% Geometry done %%%%

model.material.create('mat1');
model.material.create('mat2');
model.material.create('mat3');
model.material.create('mat4');
model.material.create('mat5');
model.material('mat1').selection.set([1]);
model.material('mat2').selection.set([2]);
model.material('mat3').selection.set([3]);
model.material('mat4').selection.set([4]);
model.material('mat5').selection.set([5 6 7 8]);

model.material('mat1').propertyGroup('def').set('electricconductivity',
{'.0002'});
model.material('mat1').propertyGroup('def').set('relpermittivity', {'1150'});
model.material('mat2').propertyGroup('def').set('electricconductivity',
{'.03'});
model.material('mat2').propertyGroup('def').set('relpermittivity', {'500'});
model.material('mat3').propertyGroup('def').set('electricconductivity',
{'.45' '0' '0' '0' '.2' '0' '0' '0' '.2'});
model.material('mat3').propertyGroup('def').set('relpermittivity', {'70e3'
'0' '0' '0' '55e3' '0' '0' '0' '55e3'});
model.material('mat4').propertyGroup('def').set('electricconductivity',
{'.0035'});
model.material('mat4').propertyGroup('def').set('relpermittivity', {'300'});
model.material('mat5').propertyGroup('def').set('electricconductivity',
{'5e5'});
model.material('mat5').propertyGroup('def').set('relpermittivity', {'1'});
```

```
model.physics('ec').feature.create('bcs1', 'BoundaryCurrentSource', 2);
model.physics('ec').feature('bcs1').set('Qjs', 1, BCrntSrc);    %Boundary
current source
model.physics('ec').feature('bcs1').selection.set(crntFace);
model.physics('ec').feature.create('gnd1', 'Ground', 2);
model.physics('ec').feature('gnd1').selection.set(grndFace);

%%Study
model.study.create('std1');
model.study('std1').feature.create('freq', 'Frequency');
model.study('std1').feature('freq').activate('ec', true);
model.study('std1').feature('freq').set('plist', '50000*1^range(1,1)');

model.mesh.create('mesh1', 'geom1');
model.mesh('mesh1').autoMeshSize(4);
model.mesh('mesh1').run;

model.sol.create('sol1');
model.sol('sol1').study('std1');
model.sol('sol1').feature.create('st1', 'StudyStep');
model.sol('sol1').feature('st1').set('study', 'std1');
model.sol('sol1').feature('st1').set('studystep', 'freq');

model.sol('sol1').feature.create('v1', 'Variables');
model.sol('sol1').feature('v1').set('control', 'freq');
model.sol('sol1').feature.create('s1', 'Stationary');
model.sol('sol1').feature('s1').feature.create('p1', 'Parametric');
model.sol('sol1').feature('s1').feature.remove('pDef');
model.sol('sol1').feature('s1').feature('p1').set('pname', {'freq'});
model.sol('sol1').feature('s1').feature('p1').set('plistarr',
{'50000*1^range(1,1)'});
model.sol('sol1').feature('s1').feature('p1').set('plot', 'off');
model.sol('sol1').feature('s1').feature('p1').set('probesel', 'all');
model.sol('sol1').feature('s1').feature('p1').set('probes', {});
model.sol('sol1').feature('s1').feature('p1').set('control', 'freq');
model.sol('sol1').feature('s1').set('control', 'freq');
model.sol('sol1').feature('s1').feature.create('fc1', 'FullyCoupled');
model.sol('sol1').feature('s1').feature.create('i1', 'Iterative');
model.sol('sol1').feature('s1').feature('i1').set('prefuntype', 'left');
model.sol('sol1').feature('s1').feature('i1').set('maxlinit', 10000);
model.sol('sol1').feature('s1').feature('i1').set('linsolver', 'bicgstab');
model.sol('sol1').feature('s1').feature('i1').set('rhob', 400);
model.sol('sol1').feature('s1').feature('fc1').set('linsolver', 'i1');
model.sol('sol1').feature('s1').feature('i1').feature.create('mg1',
'Multigrid');
model.sol('sol1').feature('s1').feature('i1').feature('mg1').set('prefun',
'gmg');
model.sol('sol1').feature('s1').feature('i1').feature('mg1').set('iter', 2);
model.sol('sol1').feature('s1').feature('i1').feature('mg1').set('mgcycle',
'v');
model.sol('sol1').feature('s1').feature('i1').feature('mg1').set('mcasegen',
'any');
model.sol('sol1').feature('s1').feature('i1').feature('mg1').set('gmglevels',
1);
model.sol('sol1').feature('s1').feature('i1').feature('mg1').set('scale', 2);
```

```
model.sol('sol1').feature('s1').feature('i1').feature('mg1').set('massem',
true);
model.sol('sol1').feature('s1').feature('i1').feature('mg1').set('mkeep',
false);
model.sol('sol1').feature('s1').feature('i1').feature('mg1').set('rmethod',
'longest');
model.sol('sol1').feature('s1').feature('i1').feature('mg1').set('mglevels',
5);
model.sol('sol1').feature('s1').feature('i1').feature('mg1').set('maxcoarsedo
f', 5000);
model.sol('sol1').feature('s1').feature('i1').feature('mg1').set('amgauto',
3);
model.sol('sol1').feature('s1').feature.remove('fcDef');
model.sol('sol1').attach('std1');

model.sol('sol1').runAll;
p=mphgetcoords(model,'geom1','domain',7);
pot1=mphinterp(model,'V','coord',[6.357;5.12+SFat+.53;0],'complexout','on');
pot2=mphinterp(model,'V','coord',[p(1);p(2);p(3)],'complexout','on');
clear p;
end
```

Matlab code for the genetic algorithm condition

```
function perChng=abc(angl2)
angl1=0;
SFat=[0.5 1.5];
BCrntSrc=6.59*(360/(angl2-angl1));
res=zeros(1,2);
for i=1:length(SFat)
    [pot1,pot2]=model_fn(SFat(i),BCrntSrc,angl1,angl2);
    res(i)=abs(imag(pot1-pot2)*1000);
end
y=abs(res(1)-res(end))/(1.5-.5);
perChng=(y/res(1))*100
dlmwrite('D:\Result.txt',[angl2 res(1) res(2)
perChng],'newline','pc','precision','%6.4f','-append')
% mphgeom(HandModel);
end
```